EBioMedicine 33 (2018) 253–268

Contents lists available at ScienceDirect

EBioMedicine

journal homepage: www.ebiomedicine.com

Research Paper

Engineered Kidney Tubules for Modeling Patient-Specific Diseases and Drug Discovery

Valentina Benedetti [a,1], Valerio Brizi [a,1], Patrizia Guida [b,1], Susanna Tomasoni [a], Osele Ciampi [a], Elena Angeli [b], Ugo Valbusa [b], Ariela Benigni [a], Giuseppe Remuzzi [a,c,d], Christodoulos Xinaris [a,*]

[a] IRCCS – Istituto di Ricerche Farmacologiche 'Mario Negri', Centro Anna Maria Astori, Science and Technology Park Kilometro Rosso, 24126 Bergamo, Italy
[b] Nanomed Laboratories, Dipartimento di Fisica, Università di Genova, 16146 Genova, Italy
[c] 'L. Sacco' Department of Biomedical and Clinical Sciences, University of Milan, 20157 Milan, Italy
[d] Unit of Nephrology and Dialysis, Azienda Socio-Sanitaria Territoriale (ASST) Papa Giovanni XXIII, 24127 Bergamo, Italy

ARTICLE INFO

Article history:
Received 12 April 2018
Received in revised form 25 May 2018
Accepted 6 June 2018
Available online 3 July 2018

Keywords:
Tubule engineering
Human pluripotent stem cells
Polycystic kidney disease
Ureteric bud
Drug discovery
PAX2

ABSTRACT

The lack of engineering systems able to faithfully reproduce complex kidney structures *in vitro* has made it difficult to efficiently model kidney diseases and development. Using polydimethylsiloxane (PDMS) scaffolds and a kidney-derived cell line we developed a system to rapidly engineer custom-made 3D tubules with typical renal epithelial properties. This system was successfully employed to engineer patient-specific tubules, to model polycystic kidney disease (PKD) and test drug efficacy, and to identify a potential new pharmacological treatment. By optimizing our system we constructed functional ureteric bud (UB)-like tubules from human induced pluripotent stem cells (iPSCs), and identified a combination of growth factors that induces budding morphogenesis like embryonic kidneys do. Finally, we applied this assay to investigate budding defects in UB-like tubules derived from a patient with a *PAX2* mutation.

Our system enables the modeling of human kidney disease and development, drug testing and discovery, and lays the groundwork for engineering anatomically correct kidney tissues *in vitro* and developing personalized medicine applications.

1. Introduction

The ability to engineer key functional units of living kidneys *in vitro* faithfully and reproducibly could revolutionize experimental nephrology and pharmacology [1, 2]. Engineered tissues could be used to investigate the basic processes underlying kidney development, function and disease, for drug discovery and toxicology studies, and potentially even as therapeutic replacements for diseased organs. To this end, a plethora of 3D culture systems have been developed over the last 50 years, using embryonic kidney cells [3–5], tissue fragments [6, 7], and primary cells or immortalized cell lines [8–13], as well as whole proximal tubules [14], and these are now considered classical tools for studying kidney development and pathophysiology. However, despite producing epithelial structures that are somewhat similar to their *in vivo* counterparts, most methods still have significant limitations. Because they rely exclusively on cell-driven self-assembly and are not controlled spatiotemporally, the resulting structures are heterogeneous in size, shape and composition. Other drawbacks include the need for extensive cell culturing, ranging from several days to weeks [9, 11] and the presence of other cell types [9], tissues [7, 12] or conditioned media [11], all of which negatively affect the reproducibility, cost-effectiveness, and overall applicability of these methods. Finally, these methods have not been tested using human cells, which is essential for studying human kidney organogenesis and pathophysiology.

Recently, the generation of kidney organoids, starting with human induced pluripotent stem cells (iPSCs), has created significant opportunities for disease modeling and toxicology studies in human tissue [15–19]. However, the usefulness of organoids generated through self-organization processes is still limited by major technical problems. One is that engineering methods cannot accurately replicate organogenesis *in vitro*, due to the kidney's intricate morphology and the multiple interactions between different cell lineages -of renal and extra-renal origin- during kidney development. In fact, several anatomical deficiencies are present in self-organizing tissues, such as the complete lack of the ureteric epithelium or random formation of ureteric buds (UB), nephron-nephron connections and branching nephrons [16, 17, 19]. Although important steps toward generating more realistic kidney

* Corresponding author at: IRCCS – Istituto di Ricerche Farmacologiche 'Mario Negri' - Centro Anna Maria Astori, Department of Molecular Medicine, Laboratory of Organ Regeneration, Science and Technology Park Kilometro Rosso, Via Stezzano, 87, 24126 Bergamo, Italy.
E-mail address: christodoulos.xinaris@marionegri.it (C. Xinaris).
[1] These Authors contributed equally.

https://doi.org/10.1016/j.ebiom.2018.06.005

organoids have recently been made by making branch-competent UB [20, 21], tissues that can be applied in biomedical research have not been generated yet. For the moment, apart from toxicity tests, there is no engineering technology that can be used to model human kidney disease quantitatively and test therapeutic drug efficacy. One possible approach to bridge this methodological gap would be to directly engineer kidney-specific units with predefined shapes and cell types that could be used for biomedical screening or combined with organoid technologies to generate more realistic mini-organs.

Engineering systems with these abilities would be particularly useful for personalized drug testing and studying human diseases that affect developmental processes, which cannot currently be studied because of the scarcity of suitable human samples.

To meet these methodological needs we developed a practical 3D engineering system that enables the generation of custom-made kidney tubules, which can actually be used for disease modeling, drug testing, and studying human kidney development. First, using 3D printing technology and PDMS prototyping, we fabricated single, branched and fractal-like moulds, into which we seeded MDCK cells to grow into tubules, with structural and functional features typical of renal epithelium. By inducing cyst formation in engineered tubules pharmacologically, we modeled polycystic kidney disease (PKD) and tested different drugs' effects on cyst regression, demonstrating that 2-deoxy-D-glucose (2DG) and berberine -a compound never tested in PKD models before- displayed a robust effect on cyst regression and restored tubular lumen and epithelial organization. To confirm that our setting can be used for pre-clinical testing in human disease, we engineered tubules using epithelial cells that were derived from an autosomal dominant polycystic kidney disease (ADPKD) patient and demonstrated that 2DG and berberine had a strong anticystogenic effect in patient-specific polycystic tubules.

By further optimizing our original protocol, we generated functional human UB-like tubules using different iPSC lines that could grow *in vitro* and undergo budding morphogenesis when co-cultured with embryonic kidneys. Finally, we identified a combination of growth factors that induces human tubules to bud and ramify, and applied this assay to study developmental defects in tubules derived from a patient carrying a heterozygous *PAX2* mutation.

This engineering system is a robust, quick and efficient tool for generating custom-made, complex functional tubules, modeling PKD, and discovering new drugs, and is also useful for studying human kidney development and individual patient's genetic defects. It also lays a solid methodological groundwork for engineering anatomically correct human kidney tissues or organoids *in vitro*.

2. Materials and Methods

2.1. PDMS Scaffold Fabrication

Polydimethylsiloxane (PDMS) scaffolds (Sylgard 184 Silicone elastomer kit, Dow Corning, Midland, MI) were fabricated using a 3-step prototyping approach: design, 3D printing and replica molding. First, scaffolds were designed by using Computer Aided Design (CAD) software (Autodesk 123D® Design ©2014 Autodesk Inc.) with different geometries: (i) three scaffolds with width and depth of 1 mm: a linear one with a straight cavity, a bifurcated one with terminal 80° branching and an asymmetrical one with two 30° lateral branches extending from the central trunk; (ii) two more complex ramified and tree-like scaffolds, the latter containing a fractal-like pattern, both 0.7 mm in depth, and ranging in width from 0.7 to 0.5 mm, respectively; (iii) a multichannel scaffold containing 11 linear microchannels that were 0.4 mm in depth × 0.4 mm in width × 9 mm in length, within a miniaturized culture chamber (1 mm in depth).

3D printing technology (Professional Pico Plus39 stereolithographic 3D printer, Asiga, CA, USA) was applied to build plastic masters (Asiga PlasWhite photopolymer resin). The printer uses an upside-down system with nominal XY pixel resolution down to 39 μm and servo resolution of 250 nm. The masters were printed at 0.5 s of exposure time, with a printing speed of 0.33 cm/h and 10 μm vertical step size. After printing, masters were cleaned by rinsing with isopropyl alcohol for 5 min, washed in distilled water, dried and exposed to UV light (365 nm) (Bio-Link-BLX-365 nm, 80 W, Vilber Lourmat) for 40 min to complete curing. To facilitate the de-molding of the polymeric replicas, masters were functionalized with an oxygen plasma treatment (Tucano plasma reactor Gambetti Kenologia) and with the deposition, from vapor phase, of an anti-sticking layer of Trichloro (1H,1H,2H,2H-perfluorooctyl) silane (FOTS, 448931-10G, Sigma-Aldrich, Saint Louis, Missouri, USA). Subsequent REplica Molding (REM) steps provide several polymeric replicas starting from a single master as previously described [22]. The PDMS base and curing agent (10:1 w/w) mixture (PDMS prepolymer) was poured onto the 3D-printed masters. PDMS was then degassed using a vacuum desiccator for 20 min, and cured in an oven at 60 °C for 2 h. Next, the cured PDMS was peeled off from the master resulting in a freestanding perforated PDMS stencil (with the pattern of the master). To control the thickness of the bottom layer of the scaffold, the PDMS stencil was placed on a 20 μm-thick PDMS prepolymer layer spin-coated on a glass cover slip, and then bonded together by thermal curing. The PDMS scaffold was obtained by detaching the assembled PDMS from the glass slide. This procedure results in scaffolds with intruded patterns, open at the top, in the form of linear, ramified, and fractal-like channels with rectangular cross-sectional geometry. Before use, PDMS scaffolds are placed in a Petri dish, with the open side facing up. To take advantage of the optical properties of PDMS for microscopy [23] and enable imaging of the forming tubules during culture inside the PDMS scaffold, the thickness of the bottom layer was maintained around 20 μm. Scaffold hydrophobicity was preserved to avoid cellular attachment [24, 25] and facilitate tissue recovery from scaffolds. Scaffolds were re-used multiple times after standard sterilization.

2.2. Cell Line and Human Primary Cell Culture Conditions

Madin-Darby Canine Kidney (MDCK) type II cell line (Cat#00062107, RRID:CVCL_0424, European Collection of Cell Cultures, Salisbury, UK) was maintained in Minimum Essential Medium Eagle (MEM) (Cat#M5650, Sigma-Aldrich) supplemented with 10% Fetal Bovine Serum (FBS) (Cat#10270, Invitrogen Corporation, Carlsbad, CA, USA), 1% L-glutamine (Cat#25030024, Invitrogen), 1% penicillin and streptomycin (Pen-Strep) (Cat#15140122, Invitrogen), and cultured in standard conditions (37 °C, 5% CO_2, 20% O_2). When 80–90% confluent, MDCK were harvested using 0.25% (w/v) Trypsin–0.53 mM EDTA (25,200,056; Invitrogen) for 2 min at 37 °C and seeded at a dilution of 1:8.

Primary single cyst-derived huADPKD cells isolated from an individual donor patient were purchased from Discovery BioMed (Discovery BioMed Inc., Birmingham, AL, USA) and cultured following the provider's recommendations. Briefly, huADKD cells were grown on permeable, clear polyester filter supports (Cat#3450, Corning) in DBM RenalCyte Specialty Medium (Discovery BioMed Inc.). When 90% confluent, huADPKD cells were harvested using 0.05% (1×) Trypsin-EDTA (Cat#15400054, Invitrogen) for 2 min at 37 °C and seeded at a dilution of 1:6. Culture medium was changed every 3 days. The huADPKD cells were used for no >6 passages.

Human iPSC lines used in our experiments were derived from healthy donor somatic cells by different technologies and characterized as previously described [26, 27]. Specifically, iPSC clone IV (RRID:CVCL_IT61) was obtained from neonatal fibroblasts using STEMCCA lentivirus [27] and iPSC#16 cells were derived from peripheral blood mononuclear cells (PBMCs) through non-integrative Sendai virus [26]. Cells were maintained in mTeSR1 (Cat#05850, StemCell Technologies, Vancouver, Canada) enriched with mTeSR1 5× Supplement (StemCell Technologies) and cultured in standard conditions (37 °C, 5% CO_2, 20% O_2) on Matrigel hESC-qualified Matrix (Cat#354277, Corning, NY, USA)-coated

plates. When 80% confluent, hiPSCs were harvested using Accutase (Cat#a1110501, Invitrogen) for 4 min at 37 °C and seeded with a concentration of 4.5×10^4 cells/cm^2 in fresh mTeSR1 complete medium supplemented with 10 μM Y27632 dihydrochloride [Rho-associated protein (ROCK) inhibitor; Cat#Y0503, Sigma-Aldrich] for the first 24 h. Culture medium was changed daily. MDCK cells and hiPSC lines were tested for mycoplasma and found to be negative (N-GARDE Mycoplasma PCR Reagent set; Cat#EMK090020, EuroClone S.p.A., Milano, Italy). The huADPKD primary cells were tested for mycoplasma by DiscoveryBiomed Inc. and were negative.

2.3. Patient iPSC Generation and Characterization

Focal segmental glomerulosclerosis (FSGS)-derived iPSCs of one consenting patient were generated from PBMCs through Sendai virus-mediated reprogramming using CytoTune-iPS 2.0 Sendai Reprogramming kit (Cat#A16517, Thermo Fisher Scientific) following the manufacturer's instructions. Briefly, cells were cultured in PBMC medium upon transduction with hKOS hc-Myc and hKLF4 viral vectors. After 7 days on mouse embryonic fibroblasts, culture medium was changed to iPSC medium until the appearance of the first colonies. The iPSC colonies were adapted to grow on Matrigel hESC-qualified Matrix (Corning) in mTeSR1 complete medium (StemCell Technologies) and cultured as described above.

To characterize patient-derived iPSCs we performed immunofluorescence analysis and qRT-PCR for pluripotency marker expression, embryoid bodies (EBs) formation, and karyotype analysis. For immunofluorescence analysis, cells were fixed in 4% paraformaldehyde (PFA) (Cat#157-8, Electron Microscopy Sciences, Hatfield, PA, USA), permeabilized with 0.3% Triton X-100 (Cat#93418, Sigma-Aldrich) for 10 min, blocked with 5% bovine serum albumin (BSA) (Cat#A2153, Sigma-Aldrich) for 1 h, and incubated with the following primary antibodies: rabbit anti-NANOG (Cat#sc-33759, RRID:AB_2150401, Santa Cruz Biotechnology, Inc., Santa Cruz, CA, USA, 1:100), mouse anti-OCT4 (Cat#sc-5279, RRID:AB_628051, Santa Cruz Biotechnology, 1:100), mouse anti-TRA 1-60 (Cat#MAB4360, RRID:AB_2119183, Merck-Millipore, NJ, USA, 1:200), mouse anti-TRA 1-81 (Cat#MAB4381, RRID:AB_177638, Merck-Millipore, 1:200), rat anti-SSEA3 (Cat#sc-21703, RRID:AB_628288, Santa Cruz Biotechnology, 1:100) and mouse anti-SSEA4 (Cat#sc-21704, RRID:AB_628289, Santa Cruz Biotechnology, 1:100) over night at 4°C. Next, samples were incubated with the appropriate Alexa Fluor®-conjugated secondary antibodies (Thermo Fisher Scientific, 1:300) for 1 h at room temperature, followed by nuclear staining with 4′,6-diamidino-2-phenylindole dihydrochloride (DAPI) (Cat#D9542, Sigma-Aldrich, 1 μg/ml) for 10 min. Specification into the three germ layers was evaluated by immunostaining the EBs for mouse anti-β-Tubulin III (ectoderm marker; Cat#CBL412X, RRID: AB_1977541, Merck-Millipore, 1:100), mouse anti-α-SMA (mesoderm marker; Cat#C6198, RRID:AB_476856, Sigma-Aldrich, 1:100) and rabbit anti-GATA4 (endoderm marker; Cat#sc-9053, RRID:AB_2247396, Santa Cruz Biotechnology, 1:50). Digital images were acquired using AxioImager Z2 microscope and AxioVision 4.8 imaging software (Carl Zeiss). All images were analyzed with ImageJ.

Gene expression level of pluripotency markers was analyzed using TaqMan probes (Thermo Fisher Scientific) specific to *OCT4*, *NANOG* and *SOX2* genes (Table 1) as described below. Gene expression levels were normalized to the housekeeping gene hypoxanthine phosphoribosyltransferase 1 (*HPRT1*).

For karyotyping, metaphase spreads were prepared after treatment with 10 mg/ml Colcemid (Cat#10295892001, Roche, Basel, Switzerland) and processed for karyotype analysis, which was performed in collaboration with the Genetic Medicine Laboratory of Azienda Ospedaliera Papa Giovanni XXIII, Bergamo (Italy). Signed informed consent was obtained from the patient in accordance with the Declaration of Helsinki guidelines.

Table 1
List of TaqMan probes.

Catalogue number	Gene symbol	Description
Hs00742896_s1	*OCT4*	*H. sapiens* POU class 5 homeobox 1
Hs00602736_s1	*SOX2*	*H. sapiens* SRY (sex determining region Y)-box 2
Hs02387400_g1	*NANOG*	*H. sapiens* NANOG homeobox
Hs00610080_ml	*T*	*H. sapiens* T, brachyury homolog
Hs00232144_m1	*LHX1*	*H. sapiens* LIM homeobox 1
Hs01057416_m1	*PAX2*	*H. sapiens* paired box 2
Hs00231122_m1	*GATA3*	*H. sapiens* GATA binding protein 3
Hs04187556_m1	*HOXB7*	*H. sapiens* homeobox B7
Hs99999909_m1	*HPRT1*	*H. sapiens* hypoxanthine phosphoribosyltransferase 1
Hs02758991_g1	*GAPDH*	*H.sapiens* glyceraldehyde-3-phosphate dehydrogenase

2.4. Differentiation of iPSCs toward Ureteric Bud (UB) Progenitor-like Cells

Human cells were induced to differentiate toward UB-like cells as previously described with minor modifications [28]. When 70–80% confluent, iPSCs were treated with Dispase (Cat#07913, StemCell Technologies) for 4 min at 37 °C. Next, the colonies were dispersed to small clusters (~200–400 cells per cluster), and split onto growth-factor-reduced Matrigel (Cat#356231, Corning)-coated plates at a ratio of 1:4. After 24 h-recovery in mTeSR1 supplemented with 10 μM ROCK inhibitor (Sigma-Aldrich), cells were grown in a chemically defined basal medium [DMEM/F12 + GlutaMAX (Cat#31331028, Invitrogen), 17.5 mg/ml BSA fraction V (Cat#126579, Merck-Millipore), 17.5 μg/ml human insulin (Cat#I9278, Sigma-Aldrich), 275 μg/ml human holotransferrin (Cat#T0665, Sigma-Aldrich), 450 μM 1-thioglycerol (Cat#M6145, Sigma-Aldrich), 0.1 mM non-essential amino acids (Cat#11140050, Invitrogen), 1% Pen-Strep (Invitrogen)] supplemented with 50 ng/ml human fibroblast growth factor 2 (FGF2) (Cat#100-18B, Peprotech, NJ, USA) and 30 ng/ml human bone morphogenetic protein 4 (BMP4) (Cat#120-05, Peprotech) for 2 days. For the next 2 days, cells were exposed to basal medium supplemented with 1 μM all-trans retinoic acid (Cat#R2625, Sigma-Aldrich), 10 ng/ml human Activin A (Cat#120-14E, Peprotech) and 100 ng/ml human bone morphogenetic protein 2 (BMP2) (Cat#H00000650-Q01, Abnova Corporation, Taiwan). Differentiation medium was changed daily.

2.5. RNA Isolation and Real Time qRT-PCR Analysis

Total cellular RNA was extracted by using Trizol Reagent (Cat#15596026, Invitrogen) following the manufacturer's recommendations. Following treatment with RNase-free DNase (Cat#M6101, Promega Corporation, Madison, WI, USA) for 1 h at 37 °C, purified RNA (2.5 μg) was reverse-transcribed using SuperScript VILO cDNA synthesis kit (Cat#11754050, Invitrogen) adhering to the manufacturer's instructions. No enzyme was added to reverse transcriptase-negative controls. Expression of pluripotency, early renal and UB-related markers was evaluated by TaqMan gene expression assay on ViiA 7 Real Time PCR system (Applied Biosystems, CA, USA) using TaqMan probes (Thermo Fisher Scientific) specific to *NANOG*, *T*, *LHX1*, *PAX2*, *GATA3* and *HOXB7* genes (Table 1) according to the supplier's instructions. Gene expression levels were normalized to the housekeeping gene glyceraldehyde-3-phosphate dehydrogenase (*GAPDH*). The ΔΔCt technique was adopted to calculate cDNA content in each sample using cDNA expression of the pluripotent state (d0) as a calibrator. Three independent experiments for each iPSC line were performed and samples were analyzed in triplicate. Data are expressed as mean ± standard deviation (SD).

2.6. Tubule Engineering

Sub-confluent MDCK cells, huADPKD cells, and differentiated iPSCs were harvested using 0.25% (w/v) Trypsin–0.53 mM EDTA (Invitrogen),

0.05% (1×) Trypsin-EDTA (Invitrogen), and Accutase (Invitrogen), respectively. Cell aliquots were centrifuged at 300 x *g* for 3 min (huADPKD cells and differentiated hiPSCs) or 4 min (MDCK cells). Pellets were resuspended in 2.4 mg/ml rat tail collagen type I (Cat#354236, Corning, Corning-Costar, NY, USA) on ice, and finally seeded in the PDMS scaffold's channels by manual pipetting. In another set of experiments, huADPKD cells were resuspended in a mixture of 3.1 mg/ml Matrigel (Cat#354234, Corning) (diluted in DBM RenalCyte Specialty Medium) and 1.5 mg/ml collagen on ice, and finally seeded into the PDMS scaffolds' cavities. Optimal cell concentrations were set-up at 1.2×10^5 cells/-μl collagen and 2×10^5 cells/μl collagen for macro- and micro-scaffolds, respectively. After collagen polymerization, the appropriate culture medium was added on the scaffold surface. Tubules were cultured under static conditions for up to 2 days in a standard incubator at 37 °C with 5% CO_2 and 20% O_2; as previously shown, these conditions allow oxygen to reach the collagen-embedded cells through passive diffusion from ambient air throughout the collagen [29]. Culture media were: DMEM/F12 + GlutaMAX supplemented with 1% FBS (Invitrogen), 1% Pen-Strep and 40 ng/ml hepatocyte growth factor (HGF) (Cat#100-39, PeproTech) for MDCK tubules; DMEM/F12 + GlutaMAX supplemented with 1% FBS (Invitrogen), 1% Pen-Strep and 40 ng/ml HGF, or DBM RenalCyte Specialty Medium for huADPKD tubules; basal medium supplemented with 1% FBS, 40 ng/ml HGF and 100 ng/ml glial cell-derived neurotrophic factor (GDNF) (Cat#ab73450, Abcam, Cambridge, UK) for iPSC-derived tubules. Bright-field images of cultured tubules were obtained using Leica ZOOM 200 stereomicroscope (Leica) and Primo Vert inverted microscope (Carl Zeiss).

2.7. Histological and Immunofluorescence Staining

For histological analysis, engineered tubules were fixed in 4% PFA for 10 min, submerged in a solution of 1:6 diluted hematoxylin (Cat#05-M06012, Bio-Optica, Milan, Italy) for 5 min, washed in distilled water and soaked in a solution of 1:9 diluted eosin (Cat#05-M10002, Bio-optica) for 1 min. Subsequently, samples were washed and mounted with Ready-to-use Dako Faramount Aqueous Mounting Medium (Cat#S3025, DAKO Corporation, Carpinteria, CA, USA), and observed by light microscopy. Concerning cross-sectional histological analysis, fixed tubules were stained with hematoxylin as previously described with minor modifications [4, 5]. Briefly, tubules were embedded in Optimal Cutting Temperature (OCT) compound (Cat#4583, Tissue-Tek, Sakura Finetek, Japan) and frozen. Next, 3-μm tubule cryosections were stained with Harris's hematoxylin (Cat#05-M06004, Bio-optica) for 2 min, mounted and observed by light microscopy. Digital images were acquired using AxioImager Z2 microscope and AxioVision 4.8 imaging software (Carl Zeiss).

Immunofluorescence analysis was performed as previously described [4, 5]. Briefly, after permeabilization in 100% cold methanol for 10 min, tubules were incubated with the following primary antibodies: mouse anti-E-cadherin (Cat#610182, RRID:AB_397581, BD Biosciences, CA, USA, 1:100), rabbit anti-podocalyxin (Cat#NB110-41503, RRID: AB_805568, Novus Biologicals, Littleton, CO, USA, 1:80), rabbit anti-PKC-ζ (C-20) (Cat#sc-216, RRID:AB_2300359, Santa Cruz Biotechnology, 1:100), rabbit anti-cleaved caspase-3 (Asp175) (5A1E) (Cat#9664, RRID:AB_2070042, Cell Signaling Technology, MA, USA, 1:200), rabbit anti-PAX2 (Cat#71-6000, RRID:AB_2533990, Thermo Fisher Scientific, 1:50), rabbit anti-Ret (C31B4) (Cat#3223, RRID: AB_2238465, Cell Signaling Technology, MA, USA, 1:100), mouse anti-HOXB7 (Cat#MAB8040, RRID:n/a, R&D Diagnostic Systems, MI, USA, 1:50), rabbit anti-Claudin 7 (Cat#E10590, RRID:AB_1660949, Spring Bioscience, CA, USA, 1:80), and goat anti-GATA3 (Cat#AF2605, RRID: AB_2108571, R&D Diagnostic Systems, 1:40) overnight at 4 °C. After washing, tubules were incubated with the appropriate secondary antibodies (Jackson ImmunoResearch Labs, West Grove, PA, USA, 1:50–1:80) overnight at 4 °C. Washed samples were soaked in DAPI (Sigma-Aldrich) for 10 min to label cell nuclei and mounted with Dako Fluorescence Mounting Medium (Cat#S3023, DAKO Corporation). For the immunostaining of 3-μm cross-sections, samples were permeabilized with 0.3% Triton X-100 for 5 min, blocked with 1% BSA for 30 min, and incubated overnight at 4 °C with primary antibodies. Subsequently, sections were incubated with the appropriate secondary antibodies (Jackson ImmunoResearch Laboratories, Inc., PA, USA, 1:50) for 2 h at room temperature, followed by nuclear staining with DAPI for 10 min. In some cases, samples were further labeled with wheat germ agglutinin-lectin (WGA-lectin) (Cat#FL-1021, Vector Labs, Burlingame, CA, USA, 1:400) for 15 min or peanut agglutinin-lectin (PNA-lectin) (Cat#RL-1072, Vector Labs, 1:80) for 90 min. Negative controls were obtained by omitting primary antibodies on adjacent sections. Finally, slides were mounted and examined. For immunofluorescence analysis of cross-sections of microtubules, fixed samples were permeabilized with cold 100% methanol for 10 min, washed and incubated in DAPI containing WGA-lectin for 15 min. After washing, tubules were embedded in OCT compound and frozen in dry ice. Next, 3-μm tubule cryosections were observed. Digital images were acquired using the LS 510 Meta inverted confocal laser scanning microscope and LSM Image browser (Carl Zeiss) and only for data shown in Fig. 4a–c and e–g, Fig. 5i,j, and for Supplementary Fig. 4a–c, Supplementary Fig. 6b and Supplementary Fig. 7c digital images were acquired using a Nikon Eclipse T*i* A1 inverted laser scanning confocal microscope (Nikon, Tokyo, Japan). Images were analyzed with ImageJ or Fiji.

For functional studies, tubules were soaked in phosphate buffered saline (PBS) containing 25 mg/ml 10-KDa fluorescence isothiocyanate-conjugated (FITC)-conjugated dextran (Cat#FD10S, Sigma-Aldrich) or 2 mM 6-Carboxyfluorescein (6CF) (Cat#C0662, Sigma-Aldrich) alone or in combination with 2 mM probenecid (Cat#P8761, Sigma-Aldrich) for 1 h at 37 °C. Following washes with ice-cold PBS, tubules were fixed and processed for immunofluorescence analysis as described above.

2.8. Tubule 3D Reconstruction

Digital z-stack images of WGA-lectin-labeled microtubules were acquired with the LS 510 Meta inverted confocal laser scanning microscope (Carl Zeiss) and were reconstructed into a 3D image through AxioVision 4.8 imaging software (Carl Zeiss).

2.9. Cyst Formation and Drug Testing in 3D Culture Systems

2.9.1. MDCK Cell-Derived Tubules

At 2 days, microtubules were harvested from PDMS scaffolds, and transferred onto polyester Transwell membranes (0.4 μm pore size; Cat#CC3460, Corning-Costar, MA, USA) containing 200 μl of 2.4 mg/ml rat tail collagen type I. Following collagen polymerization (45 min at 37 °C), 1.5 ml of culture medium, composed of MEM supplemented with 10% FBS (Invitrogen), 1% L-glutamine and 1% Pen Strep, was added. Samples were cultured for 7 days in the presence of the following agents at doses that were selected on the basis of previous studies: 10 μM forskolin [30] (Cat#F6886, Sigma-Aldrich), then for another 7 days with 10^2 μM Octreotide acetate (OCTR) [31] (Cat#0239950, Toronto Research Chemicals, Brisbane Rd., North York, Canada), 10^2 μM Pasireotide diaspartate (PAS) [31] (kind gift from Novartis Farma S.p. A., Varese, Italy), 10^4 μM 2-Deoxy-D-glucose (2DG) [32] (Cat#D6134, Sigma-Aldrich), 10 μg/ml berberine chloride [33] (Cat#B3251, Sigma-Aldrich), 0.5 μM Rapamycin [34] (Cat#R0395, Sigma-Aldrich), or 10^{-2} μM Arginine Vasopressin (AVP) (Cat#V9879, Sigma-Aldrich) alone or in combination with 10^{-2} μM Tolvaptan [35] (Cat#T7455, Sigma-Aldrich). For OCTR and PAS dosing, we based this on data from Masyuk et al. [31] to optimize the best dosage for our system. Control samples were maintained in culture medium alone for 14 days.

2.9.2. HuADPKD Cell-Derived Tubules

At 2 days, huADPKD microtubules engineered in (i) collagen or (ii) collagen and Matrigel mixture were harvested from PDMS scaffolds,

and transferred onto polyester Transwell membranes containing 200 μl of 2.4 mg/ml rat tail collagen type I or 6.2 mg/ml Matrigel, respectively. For the condition (i), following collagen polymerization (45 min at 37 °C), 1.5 ml of culture medium (DMEM/F12 + GlutaMAX supplemented with 1% FBS) was added. Samples were cultured for 2 days in the presence of 10 μM forskolin and for another 2 days in the presence of 10^4 μM 2DG or 10 μg/ml berberine chloride. Control samples were stimulated with forskolin for 2 days and then maintained in culture medium for additional 2 days.

For the condition (ii), following Matrigel polymerization (45 min at 37 °C), 1.5 ml of culture medium (DBM RenalCyte Specialty Medium) was added. Samples were cultured for 2 days with the culture medium alone, and for another 3 days in the presence of 10^4 μM 2DG or 10 μg/ml berberine chloride. Control samples were maintained in culture medium alone for 5 days.

Culture media were changed every 2 days. Finally, tubules were harvested, fixed in 4% PFA and processed for immunofluorescence analysis or hematoxylin and eosin staining as described above. The number of cysts of hematoxylin and eosin-stained tubules were quantified. The area of each field was calculated using AxioVision 4.8 software. Data are expressed as number of cysts/mm^2. Forskolin, rapamycin, Tolvaptan and berberine chloride were reconstituted in dimethyl sulphoxide (DMSO) (Cat#D2650, Sigma-Aldrich). OCTR and PAS was reconstituted in sterile saline solution. AVP and 2DG were resuspended in sterile distilled water. Once in solution, the compounds were diluted in culture medium. The final DMSO concentration never exceeded 0.1%.

2.9.3. Preliminary Experiments for the Optimization of Spontaneous Cystogenesis

In a first set of experiments, huADPKD cells were resuspended in 6.2 mg/ml Matrigel, seeded into the PDMS microscaffolds and cultured for 2 days with DBM RenalCyte Specialty Medium. Tubules were then cultured in the 3D Matrigel system with the same medium for 5 days. In a second set of experiments, huADPKD cells were resuspended in 2.4 mg/ml collagen, seeded into the PDMS micro-scaffolds and cultured for 2 days with DMEM/F12 + GlutaMAX supplemented with 1% FBS and 40 ng/ml HGF. Tubules were then cultured in the 3D Matrigel system with the same medium for 8 days.

2.10. 3D Culture Experiments for Human Developmental Study

At 2 days, fragments of about 0.6 mm in width × 4.0 mm in length of iPSC-derived macrotubule were transferred to polyester Transwell membranes as described above. Embryonic day (E) 13.5 CD1 mouse (Charles River Italia S.p.A., Calco, Lecco, Italy) kidneys were freshly isolated as previously described [4, 5]. For co-culture experiments, four E13.5 kidneys were placed in close proximity to - but not in contact with - each tubule and, after collagen polymerization, culture medium [Advanced DMEM (Cat#12491023, Invitrogen) supplemented with 2% embryonic stem cell FBS (Cat#16141079, Invitrogen), 1% L-glutamine and 1% Pen-Strep] was added. Other samples were cultured in Advanced DMEM supplemented with 1 μg/ml heparin (VERACER, Medic Italia S.r.l., Roma, Italy) and different combinations of the following growth factors: 40 ng/ml HGF (Cat#100-39, PeproTech), 100 ng/ml GDNF (Cat#ab73450, Abcam), 200 ng/ml FGF1 (Cat#100-17A, PeproTech) and 100 ng/ml FGF7 (Cat#100-19, PeproTech). Cultures were monitored by light microscopy for up to 2 days without changing the medium. The overall budding events were quantified in bright-field images of UB-like tubules. Data are expressed as percentage of ramified buds over total buds that emerged from human tubules.

The IRCCS – Istituto di Ricerche Farmacologiche Mario Negri adheres to the principles set out in the following laws, regulations, and policies governing the care and use of laboratory animals: Italian Governing Law (D.lgs 26/2014; Authorization n.233/2010-A issued December 21, 2010 by Ministry of Health); Mario Negri Institutional Regulations and Policies providing internal authorization for persons conducting animal experiments (Quality Management System Certificate – UNI EN ISO 9001:2008 – Reg. N° 6121); the NIH Guide for the Care and Use of Laboratory Animals (2011 edition) and EU directives and guidelines (EEC Council Directive 2010/63/UE). The Statement of Compliance (Assurance) with the Public Health Service (PHS) Policy on Human Care and Use of Laboratory Animals has been recently reviewed (9/9/2014) and will expire on September 30, 2019 (Animal Welfare Assurance #A5023-01).

2.11. General Methods and Statistical Analysis

The sample size was estimated to be at least 3 samples per group to detect the expected difference with an 80% power (unpaired *t*-test, two-sided; $\alpha = 0.05$), based on a previous study [36] showing that forskolin induced 150 ± 30 (mean ± SD) cysts/well compared to control. Samples were randomly allocated to the experimental groups and no inclusion or exclusion criteria were used. Quantification analyses were performed in a double-blind fashion by two investigators. Statistical analysis was performed using GraphPad Prism software (GraphPad, San Diego, CA, USA). When two conditions were compared, two-tailed Student's *t*-test [$t = 6.209$, DF = 11 (for cyst quantification); $t = 12.06$, DF = 4 (for ramified over total buds quantification)] was used. When more than two conditions were compared, one-way ANOVA with Tukey's multiple comparisons test [F = 38.17, F (DFn, DFd): 3.536 (5, 50) (for cyst quantification in MDCK experiments); F = 49.24, F (DFn, DFd): 7.727 (2, 33) and F = 200.6, F (DFn, DFd): 1.722 (2, 62), for cyst quantification in huADPKD experiments (Fig. 4D and H, respectively)] and Holm-Sidak's multiple comparisons test [F = 8.889, F (DFn, DFd): 0.5217 (4, 10) (for ramified over total buds quantification)] were used. Differences were considered to be significant when $P < 0.05$. Data are expressed as means ± standard error of the mean (SEM). See figure legends for details on number of replicates and *n* values used.

3. Results

3.1. Design and Fabrication of 3D-Printed Scaffolds

Based on the structure of the UB tree [37], we developed three basic patterns shaped to resemble UB segments: a straight line (Fig. S1A) for UB trunks, a terminal 80° bifid branch (Fig. S1B) and asymmetric lateral 30° branches (Fig. S1C) for UB ramifications. To mimic segments of UB branches in advanced stages of development, we merged the basic 80° and 30° schemes into a ramified pattern (Fig. S1D). Next, to quickly and routinely design fractal-like ramifications similar to those observed in early kidney development [37], we developed a 'golden fractal tree' (GFT) formula (Fig. S1E) that, unlike previously described GFTs with constant amplitude [38, 39], allows progressive narrowing of bifurcations an infinite number of times, avoiding branch overlapping (Fig. S1F). Finally, to engineer numerous tubules simultaneously, we designed a linear multichannel pattern (Fig. S1G).

Then we converted custom-designed patterns into plastic masters using rapid prototyping technologies and 3D printing, and used them as moulds to produce PDMS replicas (Figs. 1A S1H and S1I). We refer to the replicas with bigger, linear and ramified shapes as 'macro-scaffolds', and those with multichannels as 'micro-scaffolds'.

3.2. Engineering Differently Shaped Tubular Structures by Seeding PDMS Scaffolds with Epithelial Cell Suspensions

To construct epithelial tubules, 0.7–6.5 × 10^5 MDCK cells/μl collagen were cultured in PDMS moulds for up to 2 days (Figs. 1B and S2A, and Methods Videos 1 and 2). To stimulate tubulogenesis, we supplemented culture medium with 40 ng/ml HGF, a strong inducer of *in vitro* branching tubulogenesis [9–11].

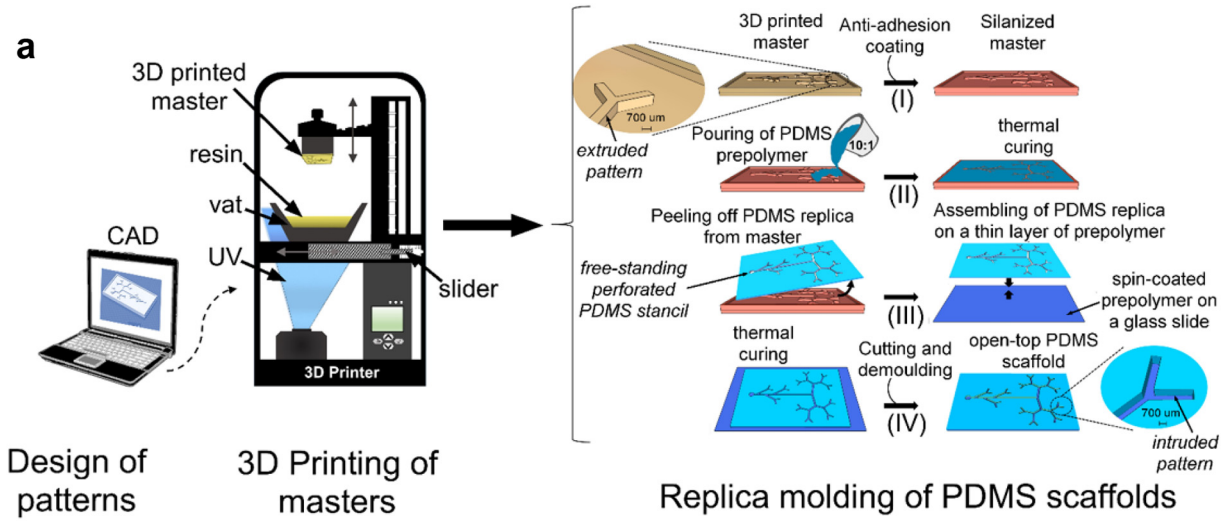
a
3D printed master
resin
vat
UV
CAD
slider
3D Printer
3D printed master
Anti-adhesion coating
Silanized master
700 um
extruded pattern
Pouring of PDMS prepolymer
10:1
thermal curing
(I)
(II)
Peeling off PDMS replica from master
Assembling of PDMS replica on a thin layer of prepolymer
free-standing perforated PDMS stancil
spin-coated prepolymer on a glass slide
(III)
thermal curing
Cutting and demoulding
open-top PDMS scaffold
(IV)
700 um
intruded pattern
Design of patterns
3D Printing of masters
Replica molding of PDMS scaffolds

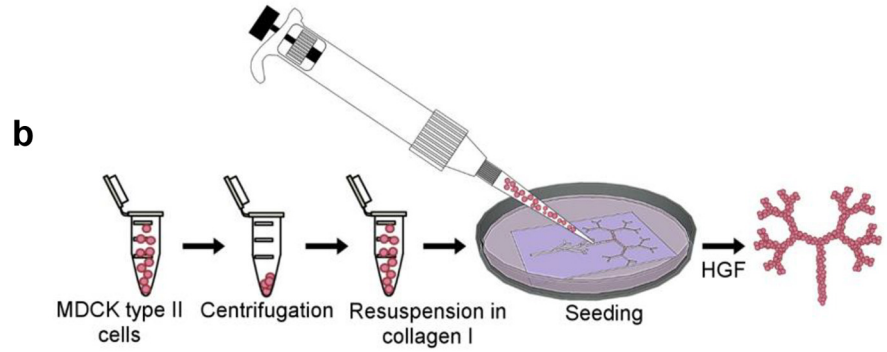
b
MDCK type II cells
Centrifugation
Resuspension in collagen I
Seeding
HGF

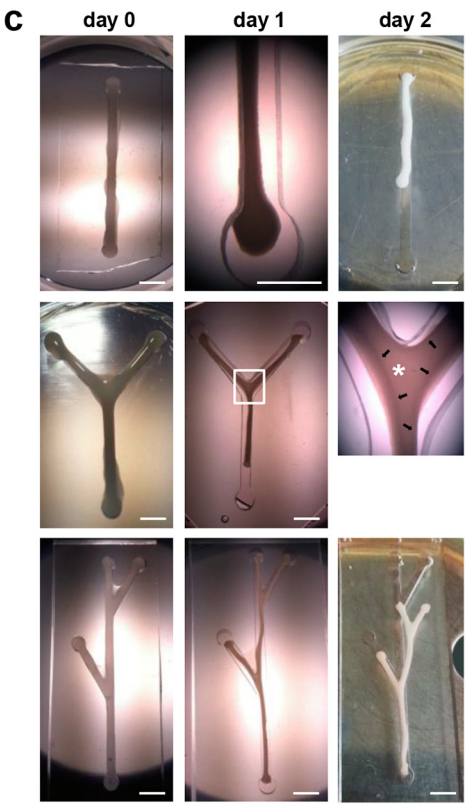
c
day 0
day 1
day 2


d


e

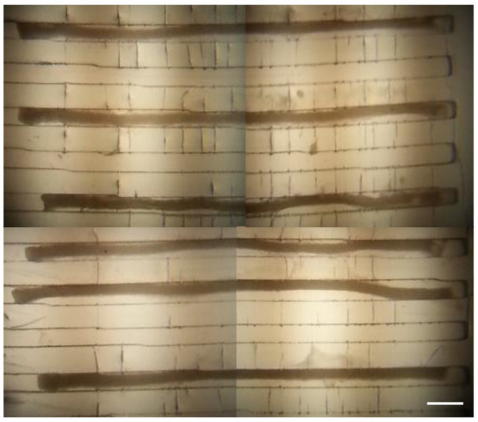
f

The seeding conditions with the highest rate of tubule formation (94% of total seeded scaffolds) were 1.2×10^5 and 2×10^5 cells/μl collagen for macro- and micro-scaffolds, respectively (Figs. 1C–F). Other cell concentrations resulted in cells clustering inside the scaffolds without developing tubules (Figs. S2B and S2C).

Three hours after seeding, dispersed cells self-organized to form tubular structures corresponding to the size and shape of the mould cavity (Fig. S2D). At 1 day, single and branched structures shrank markedly and began detaching from the moulds (Fig. 1C). At 2 days, whole intact branches emerged autonomously from the cavity (Fig. 1C). Remarkably, a luminal space was visible through bright-field microscopy as a translucent region delimited by darker edges at bifid branching points, suggesting a common cavity between tubular structures was forming (Fig. 1C).

Depending on scaffold size, we refer to the tubular structures generated in Figs. 1C–F as 'macrotubules' (both single and in networks) and 'microtubules', respectively.

3.3. Engineered Tubules Undergo Rapid Lumen Formation and Epithelial Polarization and Exhibit Macromolecule and Organic Anion Transport Capacity

Lumenogenesis is a critical step in tubule formation and involves epithelial rearrangement and polarity establishment [40]. Confocal z-stack images of engineered microtubules from the surface to the inner region revealed a single lumen surrounded by a monolayer of cells positive for E-cadherin, a transmembrane glycoprotein that plays an important role in the establishment of cell-cell adherent junctions and renal epithelial polarity [41] (Fig. 2A). Three-dimensional reconstructions of z-stack images and cross-section analysis further confirmed the presence of a luminal cavity delineated by WGA-lectin-positive cells (Fig. 2B and C). As in microtubules, branches from macrotubular systems had well-established epithelial structures with a coalesced lumen. A monolayer of cells positive for E-cadherin in the lateral membrane, and WGA-lectin in the basement membrane, lined the tubular walls (Fig. 2D). Some cells were also positive for PNA-lectin [42] and podocalyxin –an integral membrane protein expressed by epithelial cells in apical membranes [43] (Fig. S3A). These data indicate that tubules with apical-basal polarized epithelia had formed.

The formation of tubes from unpolarized single cells, either *in vivo* or in artificial engineering systems, can occur through cavitation or hollowing [42, 44, 45]. To provide insight into the mechanism underlying lumen formation we examined tubules at an earlier stage. At 1 day, macrotubules had a major lumen enclosed by peripheral cells that had changed morphology and displayed nuclei aligned along the tubular walls. Cells in the centre of macrotubules showed chromatin condensation (Fig. S3B) and immunoreactivity for cleaved caspase 3 –both clear signs of apoptosis. In contrast, peripheral cells showed no signs of apoptosis (Fig. S3C). These data showed that in our system the mechanism is apoptosis-mediated cavitation. In controlled experiments without HGF, phenotypically compact tubules did form, but could not develop a lumen (Fig. S3D).

To test whether engineered microtubules had functional properties, like absorbing macromolecules and transporting organic anions, we soaked them in solutions containing FITC-dextran (10 kDa) or 6-carboxyfluorescein (6CF) [46, 47]. Dextran was internalized abundantly in the central areas of the microtubule (Fig. 2E). Otherwise, no 6CF was found in central lumen areas, while E-cadherin-positive cells, confined to the tubules' surfaces, internalized 6CF and retained it in their cytoplasm (Fig. 2F). When we cultured tubules in the presence of both 6CF and the organic anion transporter (OAT) inhibitor probenecid [48], no fluorescence was detected in the cells (Fig. 2G), indicating that 6CF internalization is transporter-mediated.

3.4. Using Engineered Tubules for Polycystic Kidney Disease Modeling, Drug Testing and Discovery

To test whether engineered tubules could be used for disease modeling and drug discovery we chose to model PKD, a genetic disease in which numerous fluid-filled cysts develop within the kidney and for which there is no effective therapy [49]. To this aim we transferred microtubules to a 3D collagen culture system and treated them with forskolin, a molecule that has previously been shown to increase intracellular cAMP levels and induce cyst development, and used extensively to study cystogenesis mechanisms in various PKD models [15, 30, 50] (Fig. 3A). At 14 days, forskolin-treated tubules had numerous translucent spheroidal cysts distributed homogeneously throughout the tubule (Fig. 3B), resulting in the lumen loss (Fig. 3C). Cysts were surrounded by a monolayer of cells positive for E-cadherin in the basolateral membranes, and podocalyxin in the apical membranes, demonstrating the presence of polarized cysts within tubules (Fig. 3D). For drug testing and discovery studies, we compared the effect of compounds with different mechanisms of action on cyst regression. We therefore treated forskolin-stimulated tubules with: (i) rapamycin -an mTOR inhibitor [51]; (ii) Tolvaptan -a highly selective arginine vasopressin (AVP) receptor antagonist [52]; (iii) octreotide (OCTR) *and (iv)* pasireotide (PAS) -both somatostatin analogues that decrease intracellular cAMP levels, cell proliferation and cystogenesis *in vivo* [31]; (v) 2-deoxy-D-glucose (2DG) -a glucose analogue that inhibits glycolysis [53]; and (vi) berberine -an isoquinoline quaternary alkaloid that has an anti-proliferative effect on various cell lines mainly by arresting the G_0/G_1 phase of the cell cycle [33, 54] but has not been studied in a PKD model.

Rapamycin treatment had no significant effect on cyst numbers compared to controls (Fig. 3E and K). To test the effect of Tolvaptan, we treated forskolin-stimulated tubules with AVP alone, or in combination with Tolvaptan [35]. Treatment with AVP alone increased cyst numbers as expected [35], while the combination of AVP and Tolvaptan significantly reduced the size and number of cysts (63%) (Fig. 3F and L). OCTR and PAS decreased cyst numbers significantly (58% and 43%, respectively) compared to forskolin-treated tubules (Fig. 3G, H and K), while 2DG and berberine were the most effective drugs for cyst regression, reducing the number of cysts by 71% and 72%, respectively (Figs. 3I–K), and restricting cysts to the peripheral areas of tubules. Although Tolvaptan- OCTR- and PAS-treated tubules showed a reduction in cyst numbers to various extents, the tubular structures and lumen were still severely damaged. In contrast, 2DG and berberine restored both the central lumen and epithelial organization (Fig. 3I and J). Together these data demonstrate that engineered tubules model PKD efficiently and respond to drug treatment in a quantifiable manner, making this system a viable tool for drug testing and discovery. Furthermore, we revealed the anti-cystogenic properties of berberine in polycystic kidney tissue, making it a promising new drug with therapeutic potential for PKD treatment.

Fig. 1. Engineering tubular structures starting from MDCK cell suspensions. (A) Schematic representation of PDMS fabrication. Designed patterns are converted into 3D plastic masters using stereolithography. Subsequently, extruded patterns of the master are replicated in the PDMS scaffolds through replica molding in four basic steps: (i) masters are treated with FOTS silane to prevent the PDMS from sticking; (ii) the PDMS prepolymer is poured on the masters and allowed to cure, forming PDMS replicas; (iii) replicas are then peeled off from the masters, and bonded to a 20 μm-thick prepolymer layer by thermal curing in order to close the bottom side; (iv) after cutting and demolding, PDMS scaffolds are ready to be sterilized and used. The same technical steps are followed to generate linear or branched open-top PDMS scaffolds with rectangular cross-sectional geometry. (B) Experimental design. MDCK cells are resuspended in collagen, seeded into PDMS scaffold by pipetting, and cultured in the presence of HGF for up to 2 days. (C) Immediately after seeding, the collagen containing cells fills the scaffold channel completely (day 0). At 1 day, tubular aggregates show marked shrinkage. At 2 days, branches emerge from the cavities, and a translucent area (middle panel, asterisk) bordered by darker edges (middle panel, arrows) is visible. (D) Ramified and (E) tree-like tubular structures at 2 days. (F) A multichannel scaffold containing microtubules at 2 days. Scale bars: 2 mm (C–E), 500 μm (F).

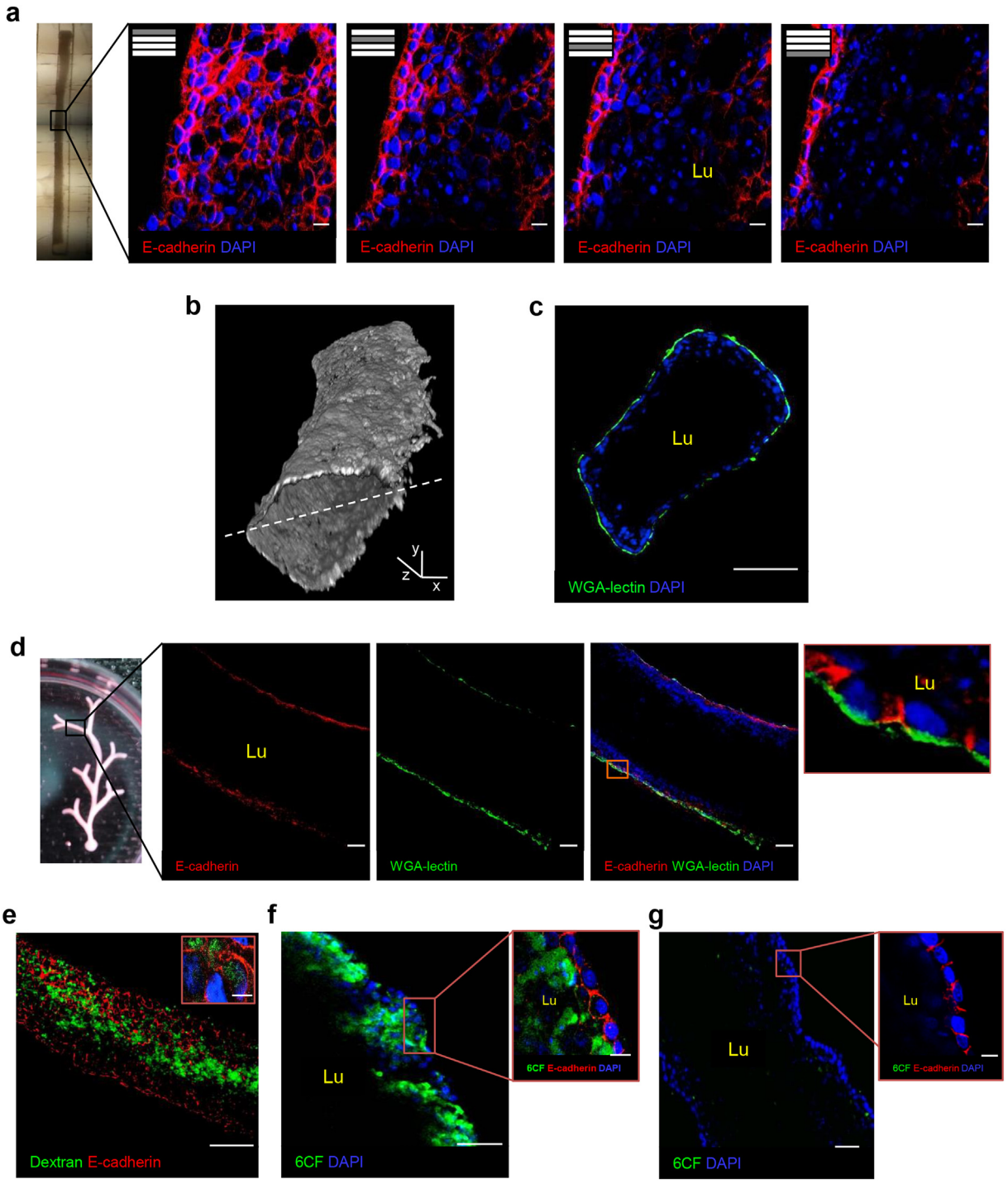

Fig. 2. Engineered tubules display lumen formation and transport function at 2 days. (A) Z-stack images of the microtubule with a single lumen (l) in the central region. E-cadherin (red) is expressed by peripheral cells of the microtubule. (B) Three-dimensional reconstruction of z-stack images of an MDCK microtubule labeled with WGA-lectin. Two distinct z-stack series of captures from the top of the tubule to its centre and from the top to the centre of the other side were reconstructed and merged into the 3D composite image. The dashed line indicates the plane of image merging. (C) Cross-section of engineered microtubule showing the lumen (Lu) enclosed by epithelial cells with aligned nuclei and positive for WGA-lectin. (D) A branch from the macrotubular system with an extended lumen (Lu) enclosed by a monolayered epithelium positive for E-cadherin (red) and WGA-lectin (green) in the lateral and basal membranes, respectively (inset). (E–G) Microtubules showing (E) dextran (green) internalization and (F) 6CF (green) anion transport in the absence or (G) presence of the organic anion transporter inhibitor probenecid. WGA-lectin, wheat-germ agglutinin-lectin; 6CF, 6-carboxyfluorescein; DAPI, blue-stained nuclei. Scale bars: 10 μm (A, E–G insets), 100 μm (D, E), 50 μm (C,F,G), x,y, 500 μm, and z, 100 μm (B).

3.5. Engineering Tubules from PKD Patient for Drug Testing and Discovery

Currently there are no patient-specific 3D models of PKD *in vitro*. To test whether our system could be used for PKD modeling and drug discovery in a patient-specific manner, we set out to generate polycystic tubules using single cyst-derived primary cells that were isolated from an individual huADPKD donor. Following identical conditions as in MDCK experiments, we engineered tubular structures (Fig. S4A) that could be cultured in 3D collagen matrix and induced by forskolin to form quantifiable cysts. Notably, after only 2 days of forskolin treatment,

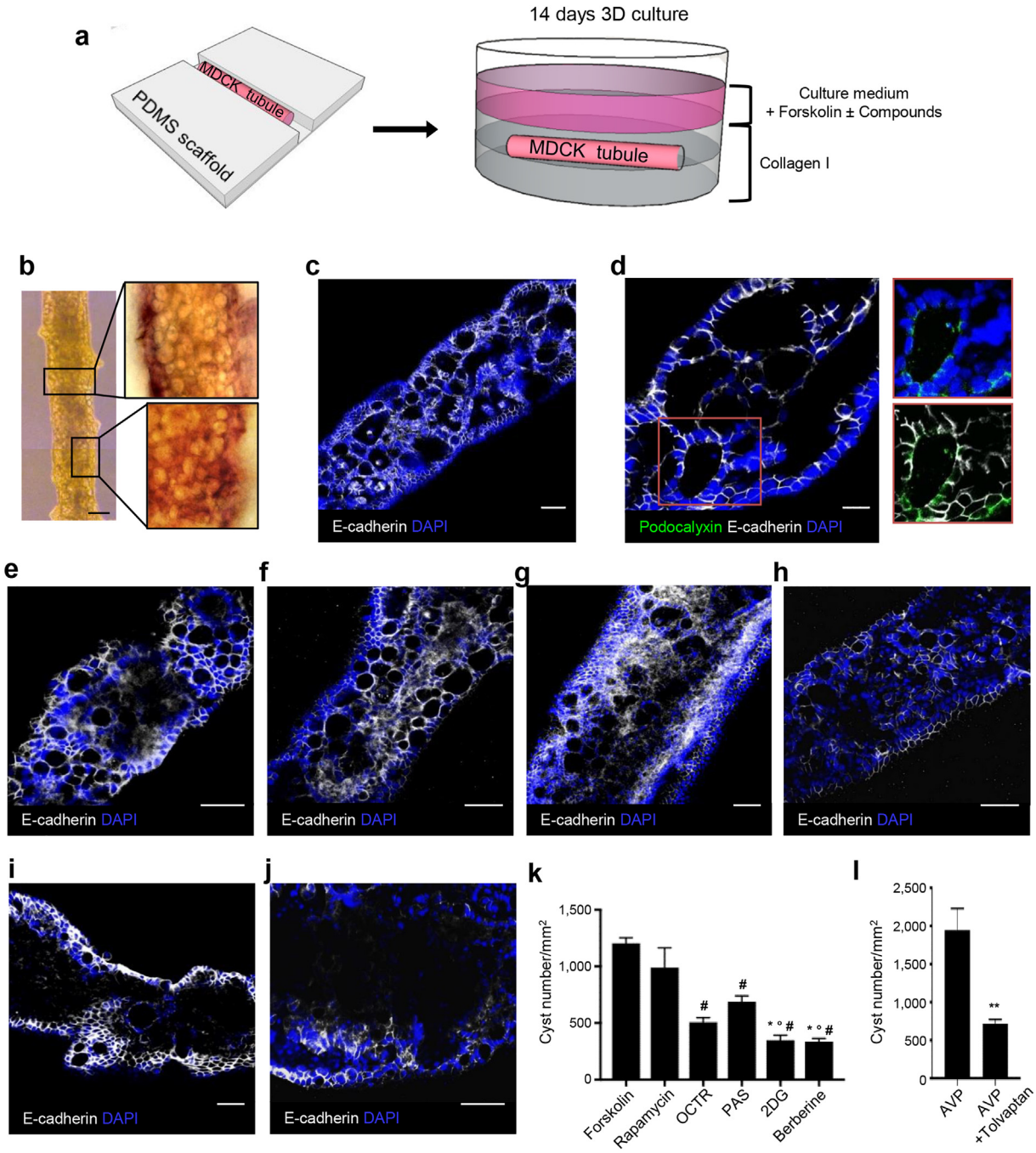

Fig. 3. MDCK-derived tubules model PKD and respond to treatment with different compounds. (A) Schematic representation of 3D collagen culture system. (B) A forskolin-stimulated microtubule showing many large spheroidal cysts stained with hematoxylin and eosin (insets). (C,D) Cysts are delimited by a monolayered epithelium positive for E-cadherin (white) in the basolateral membranes and (D) podocalyxin (green) in the apical membranes (insets). The tubular lumen is lost. (E–J) Forskolin-stimulated tubules after 7 days' treatment with (E) rapamycin, (F) Tolvaptan in combination with AVP, (G) OCTR, (H) PAS, (I) 2DG or (J) berberine. (I,J) 2DG and berberine treatments restore tubular lumen. (K,L) Quantification of cyst number/mm^2: No treatment (forskolin; 1205 ± 48.81); rapamycin (990 ± 174.5); OCTR (508.5 ± 39.52); PAS (688.9 ± 52.1); 2DG (348.1 ± 44.15); berberine (335.8 ± 27.93); AVP (1948 ± 283.4); AVP + Tolvaptan (716.4 ± 57). Data are expressed as means ± SEM from three independent experiments. (K) Number of fields analyzed: $n = 18$ for forskolin, $n = 6$ for rapamycin, $n = 6$ for OCTR, $n = 7$ for PAS, $n = 8$ for 2DG, $n = 11$ for berberine. $^{*}P < 0.05$ *versus* PAS, $^{\circ}P < 0.0001$ *versus* rapamycin, $^{\#}P < 0.0001$ *versus* forskolin by one-way ANOVA with Tukey's multiple comparisons test. (L) Number of fields analyzed: $n = 4$ for AVP, $n = 9$ for Tolvaptan in combination with AVP. $^{**}P < 0.0001$ by two-tailed Student's *t*-test. DAPI, blue-stained nuclei; AVP, arginine vasopressin; OCTR, octreotide; PAS, pasireotide; 2DG, 2-deoxy-D-glucose. Scale bars: 100 μm (B), 50 μm (C, E–J), 20 μm (D).

tubules displayed numerous cysts (Fig. 4A), resembling mature cysts in PKD patients [55, 56]. To validate whether the compounds that were found to be the most effective for cyst regression using MDCK-derived tubules could be of therapeutic value in human disease, we treated engineered huADPKD tubules with 2DG and berberine for 2 days, and evaluated cyst numbers (Figs. 4B-4D). Remarkably, both compounds showed a strong anti-cystogenic effect in patient-derived polycystic tubules by reducing the cyst number by 58% and 59%, respectively (Fig. 4D). No cysts were formed in the absence of forskolin under our standard culture conditions.

To confirm that the observed anti-cystogenic effects of 2DG and berberine were not associated with forskolin treatment *per se*, we set out to optimize the culture conditions that would allow cyst formation without the use of forskolin (Figs. S4B and S4C). Culturing patients' cells in

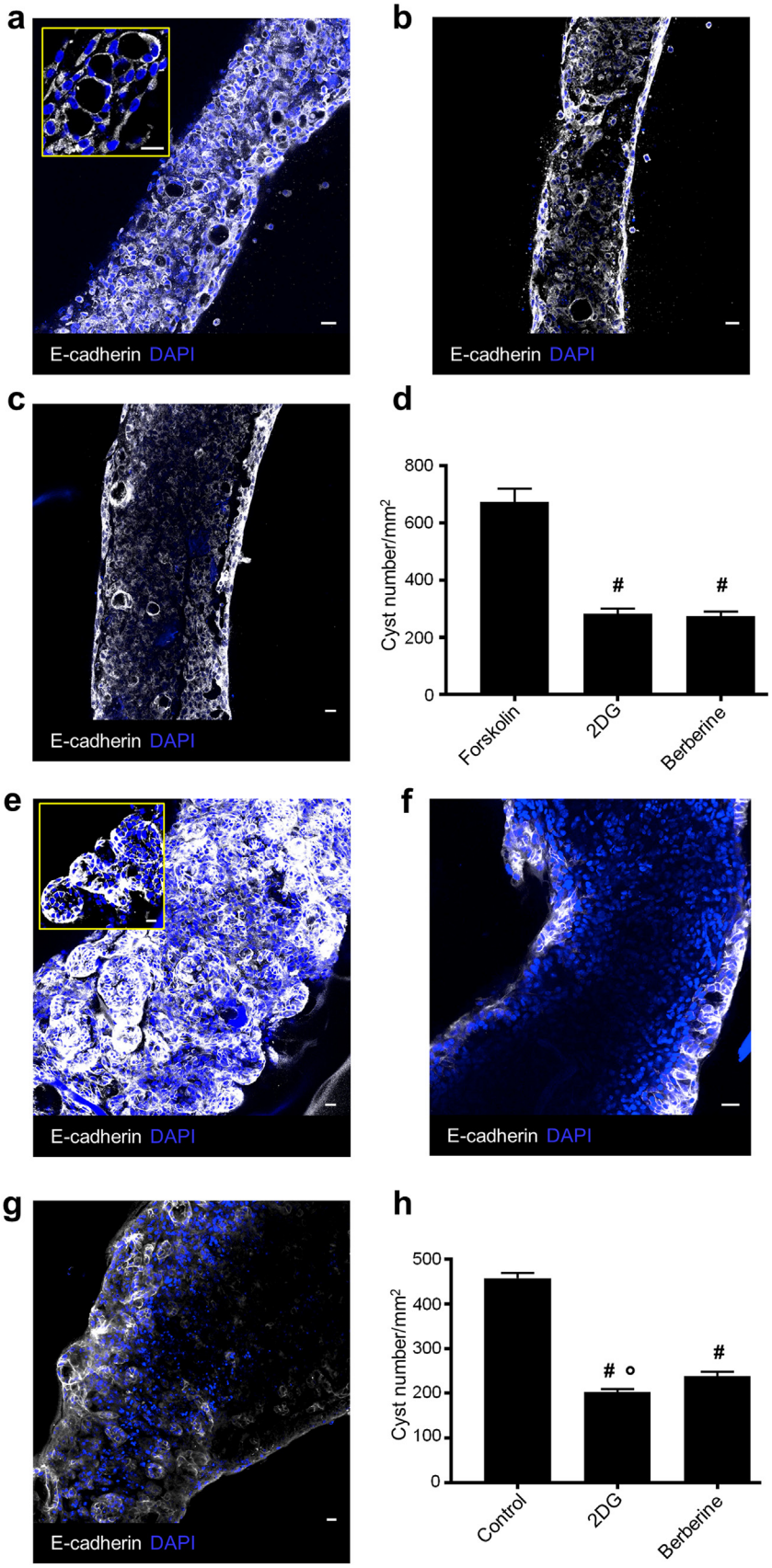
a
E-cadherin DAPI
b
E-cadherin DAPI
c
E-cadherin DAPI
d
Cyst number/mm2
800
600
400
200
0
#
#
Forskolin
2DG
Berberine
e
E-cadherin DAPI
f
E-cadherin DAPI
g
E-cadherin DAPI
h
Cyst number/mm2
500
400
300
200
100
0
°
#
Control
2DG
Berberine

a combination of matrigel and collagen in the scaffolds for 2 days, followed by 5-day culture in a 3D Matrigel system, allowed for the formation of numerous cysts (Fig. 4E), resembling early-stage cysts in PKD patients [56]. Even under these conditions, 2DG and berberine exerted a strong anti-cystogenic effect (56% and 48%, respectively) (Figs. 4F–H), further confirming the therapeutic potential of the compounds.

Overall, these findings demonstrate that our engineering system can be used to model human PKD and test drug efficacy, and can provide a reliable method for precision medicine applications. Moreover, these data highlight that our forskolin-inducible system is a reliable tool for initial preclinical drug screening and disease modeling studies.

3.6. Engineering Human UB-Like Tubules Using iPSCs

Next, we tested our system's ability to efficiently engineer human tubules, starting with iPSCs previously generated in our laboratory through lentiviral-mediated reprogramming [27]. First, we directed the differentiation of iPSCs into UB-committed renal progenitor cells through 4-day exposure to defined media conditions [28] (Fig. S5). Then we re-suspended cells obtained from 2 to 4 days of differentiation in collagen and seeded them into branched scaffolds according to the 3D culture setting and tubulogenic conditions established for MDCK cells (Fig. 5). Although 3- and 4-day cells generated compact tubular structures, exposure to HGF alone did not suffice to form epithelia endowed with a single lumen (Fig. S6A). Thus, we modified culture conditions by adding in the medium glial cell-derived neurotrophic factor (GDNF), a molecule secreted by the metanephric mesenchyme that is essential for UB formation, growth and branching during kidney development [57]. At 2 days of culture, we observed a continuous lumen in iPSC-derived tubules (Fig. 5B and C) delimited by a monolayer of cells positive for E-cadherin and WGA-lectin and the apical marker protein kinase C-ζ (PKC-ζ) [58] (Figs. 5B and S6B). Like in MDCK tubules, 3D reconstructions of z-stack images and cross-section analysis further confirmed the presence of a luminal cavity delineated by WGA-positive cells (Fig. 5D and E). Moreover, engineered tubules were positive for the UB markers PAX2, HOXB7, Claudin-7 and GATA3, as well as the ureteric tip marker Ret, which displayed a heterogeneous pattern of expression (in small groups) as occurs in primary UB development [59], indicating UB epithelium induction (Figs. 5F–L). Finally, engineered tubules showed immense amounts of dextran throughout the tubular lumen and a patchy 6CF signal in the cytoplasm of peripheral cells (Fig. 5M and N). Neither undifferentiated nor 2-day differentiated cells formed tubule-like structures (Figs. S6C and S6D).

Like MDCK tubules, at 1 day many apoptotic cells, identified by chromatin condensation and caspase 3 cleavage, were visible in the centre of macrotubules, indicating that cavitation is the mechanism of lumen formation (Figs. S6E and S6F).

To test the reproducibility of our system, we engineered tubules using a iPSC line obtained in our laboratory through Sendai virus-mediated reprogramming of peripheral blood mononuclear cells from one healthy donor [26]. After iPSC differentiation we successfully engineered UB-like tubules (Fig. S7), indicating that our system is robust and reproducible.

3.7. Using Engineered Tubules to Study Human UB Developmental Processes and Defects

Key processes of early UB morphogenesis are the budding – evagination of lateral buds from a preexisting tubular epithelium that culminate with one tip - and the clefting – division of a tip into two branches [60, 61]. To test whether engineered human tubules displayed UB developmental properties and would respond to kidney developmental signals, we co-cultured macrotubules with mouse embryonic kidneys (Fig. 6A), which have been shown to release a wide spectrum of soluble factors in organotypic cultures [62]. At 1 day, primary buds emerged from the tubule. At 2 days, lateral ramifications emerged from primary buds, forming the secondary buds (Fig. 6B). These buds consisted of aligned epithelial cells (Fig. 6C).

Next we tested the effect of different combinations of growth factors involved in UB morphogenesis [6, 57, 63, 64] on inducing tubule budding. The basal culture condition with HGF and GDNF induced 35.05 ± 1.02% of ramified buds in the total budding events (Fig. 6D). Adding Fibroblast Growth Factor (FGF) 1 [64] or FGF7 [63, 64], —strong inducers of UB cell proliferation and growth in rodents- to the basal culture condition did not increase the percentage of ramified buds significantly (41.11 ± 10.60% and 52.38 ± 6.24%, respectively). Conversely, when all growth factors were used together, the number of ramified buds increased markedly (71.96 ± 3.22%) (Figs. 6D–F) and was similar to that observed when we used mouse embryonic kidneys (74.81 ± 4.12%) (Fig. 6B and D). In some cases we also observed UB clefts where terminal bifid branching occurred (Fig. 6E, asterisks).

Since engineered tubules can recapitulate early steps of UB development, we applied our system to study possible developmental defects in UB morphogenesis using Paired box 2 (*PAX2*) mutated cells. The *PAX2* gene is highly activated in both UB and metanephric mesenchyme [65], and its heterozygous mutations lead to reductions in UB branching and nephron numbers [66]. We therefore generated iPSCs from one patient with a rare heterozygous *PAX2* mutation [67], differentiated them toward UB-like cells and then engineered patient-derived macrotubules (Figs. S8 and S9). These tubules were cultured alongside healthy donor-derived tubules, used as controls, as defined above (Fig. 6E–F, and H–I). Quantification analysis revealed a marked reduction of ramified buds in patient-derived tubules compared with controls (Fig. 6G), as can be seen *in vivo* [66, 68]. Altogether, these results clearly demonstrate that engineered tubules recapitulate early steps of UB morphogenesis, and can be used to study human developmental mechanisms and individual's genetic defects.

4. Discussion

Here we described a novel technology for engineering custom-made, complex kidney tubules, which can be used for disease modeling, drug testing, and studying human kidney development. Using a kidney-derived cell line, our method efficiently yielded tubules of different sizes and shapes endowed with a lumen and polarized cells that display transport characteristics typical of renal epithelia, and can be used for PKD modeling and drug testing. We successfully employed this system to generate patient-specific polycystic tubules and to test new drugs, confirming the robustness and reliability of our system in preclinical drug discovery and testing. By optimizing this protocol we then

Fig. 4. ADPKD patient-derived tubules develop cysts and respond to treatment with 2DG and berberine. (A) A huADPKD microtubule stimulated with forskolin in the 3D collagen culture system displaying several cysts. The tubular lumen is lost. (B,C) Forskolin-stimulated tubules after treatment with (B) 2DG and (C) berberine. Both treatments markedly reduce cyst number and promote tubular lumen re-establishment. (D) Quantification of cyst number/mm^2: no treatment (forskolin; 674.1 ± 46.1); 2DG (282.3 ± 18.5); berberine (275.3 ± 15.4). (E) A huADPKD microtubule engineered by resuspending cells in a Matrigel and collagen mixture and cultured in the 3D Matrigel system displaying several large cysts. The tubular lumen is lost. (F,G) Tubules engineered and cultured as in (E) after treatment with (F) 2DG and (G) berberine, display significantly reduced cyst numbers and a visible tubular lumen. (H) Quantification of cyst number/mm^2: no treatment (control; 457.6 ± 11.8); 2DG (202.8 ± 7.0); berberine (238.7 ± 10.0). Data are expressed as means ± SEM from three independent experiments. Number of fields analyzed: (D) $n = 14$ for forskolin, $n = 10$ for 2DG, $n = 12$ for berberine; (H) $n = 22$ for control, $n = 22$ for 2DG, $n = 21$ for berberine. $^{\#}P < 0.0001$ *versus* forskolin, $^{*}P < 0.0001$ *versus* control, $^{\circ}P < 0.05$ *versus* berberine by one-way ANOVA with Tukey's multiple comparisons test. 2DG, 2-deoxy-D-glucose; DAPI, blue-stained nuclei. Scale bar 20 μm.

generated functional hiPSC-derived-UB-like tubules, which grew and underwent budding morphogenesis when co-cultured with embryonic kidneys. Finally, we used this system to identify a combination of growth factors that induces human UB-like tubules to bud and ramify, and to study the effect of a *PAX2* mutation on budding morphogenesis, using patient-derived tubules.

Due to the MDCK cells' epithelial features [69, 70] and the ability to form individual fluid-filled cysts, when cultured in 3D ECM environments and stimulated with cAMP elevating agents, they have been used extensively to model PKD and explore drug efficacy on renal cyst development [30, 36, 71]. However, conventional 3D cell cultures have significant limitations. In particular, the formation of individual cysts

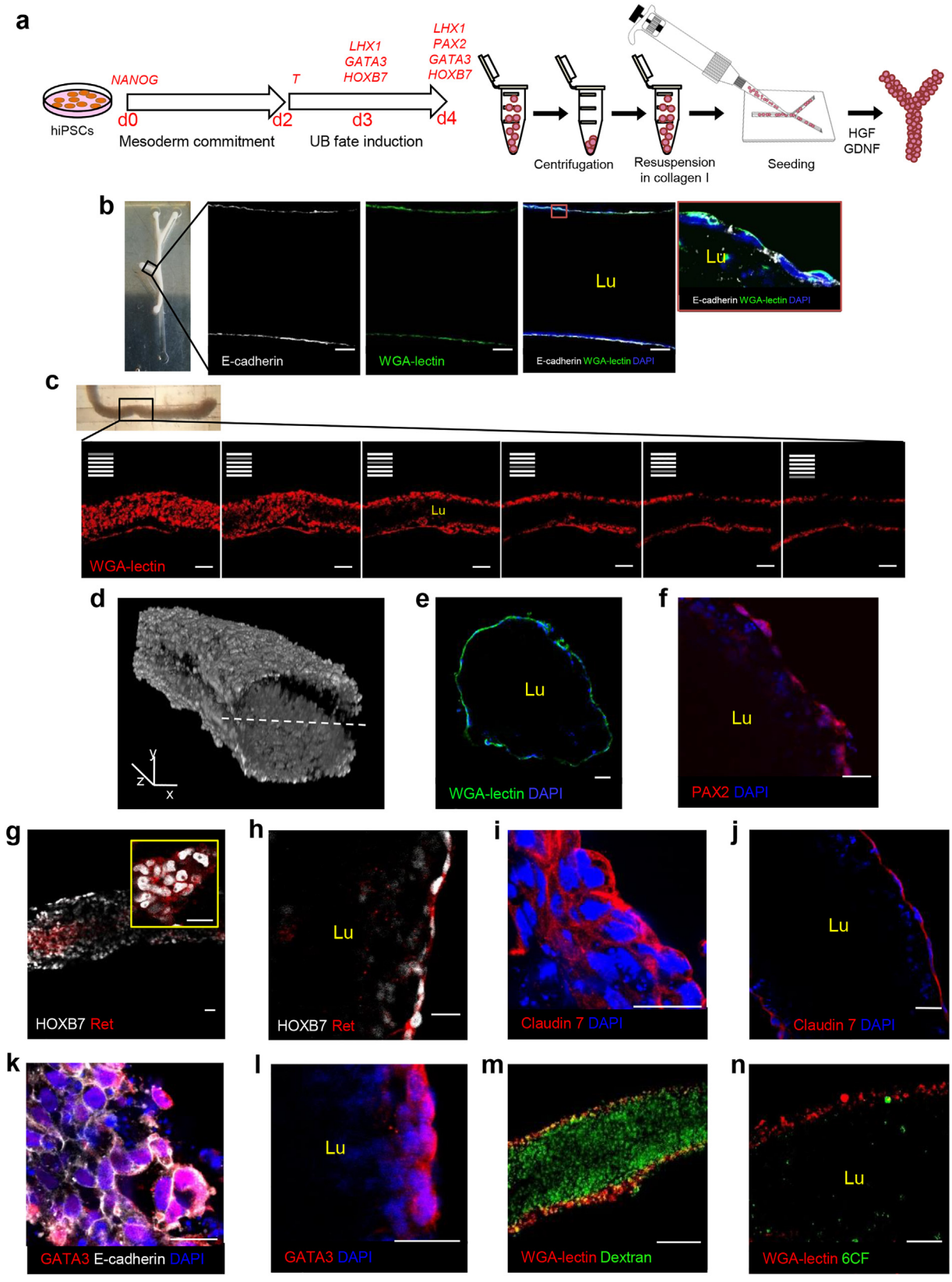

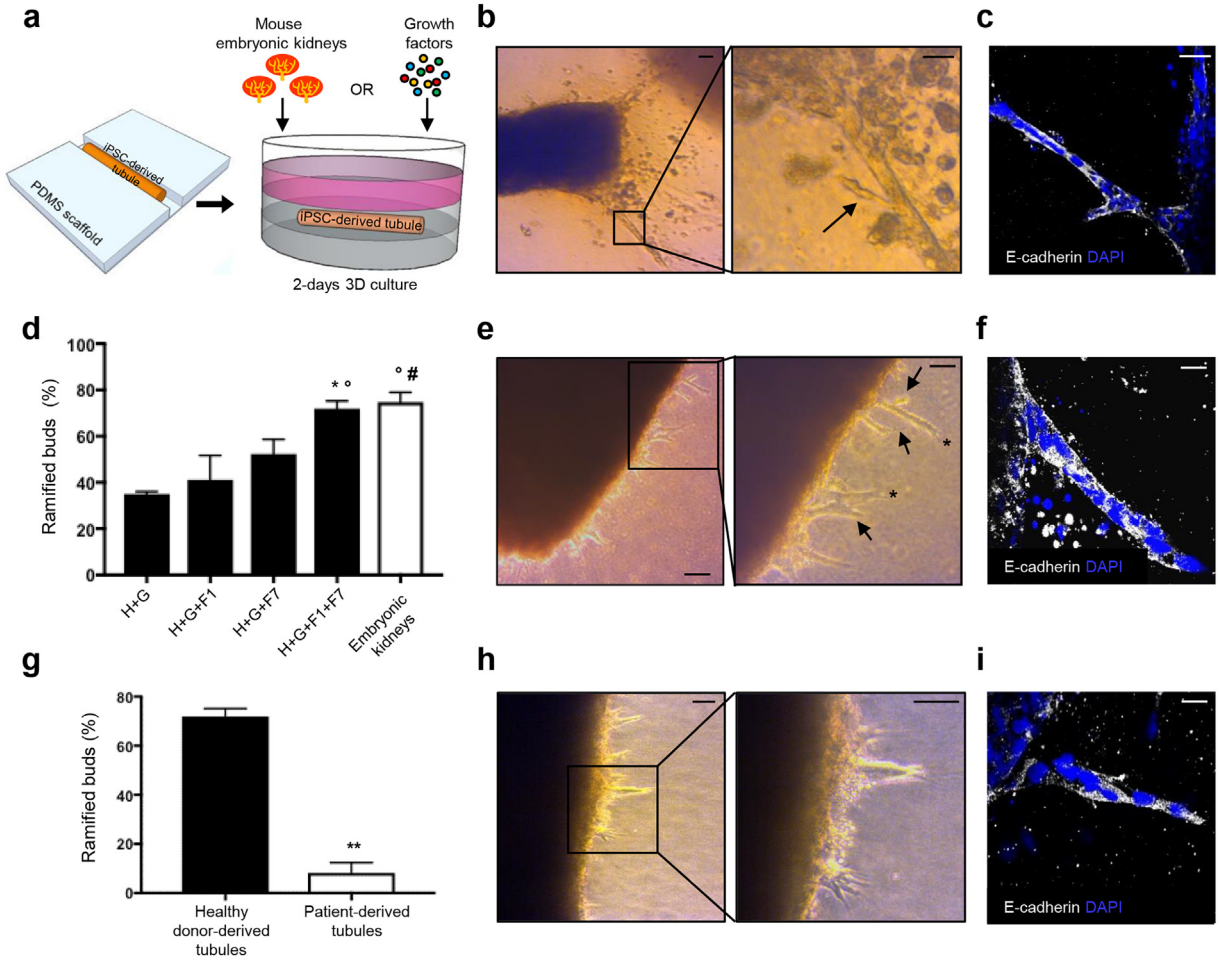

Fig. 6. Engineered tubules as a tool for studying human UB developmental processes and defects. (A) Experimental design. Fragments of iPSC-derived macrotubules are cultured with mouse embryonic kidneys or with growth factors in the 3D collagen culture system. (B,C) Healthy donor-derived tubule co-cultured with mouse embryonic kidneys. (B) At 1 day, long primary buds emerge (left panel). At 2 days, a lateral ramification (arrow) arises from the primary bud. (C) A ramified bud consists of aligned E-cadherin-positive cells (white). (D) Percentage of the ramified buds in the total buds emerged from healthy donor-derived tubules. Data are expressed as means ± SEM from three independent experiments. Number of fields analyzed: $n = 48$ for H + G, $n = 30$ for H + G + F1 and H + G + F7, $n = 22$ for H + G + F1 + F7, $n = 21$ for mouse embryonic kidneys. $^{*}P < 0.05$ *versus* H + G, $^{\circ}P < 0.05$ *versus* H + G + F1, $\#P < 0.01$ *versus* H + G by one-way ANOVA with Holm-Sidak's multiple comparisons test. (E,F) Healthy donor-derived tubule cultured with all growth factors displays primary and secondary buds (arrows) some of which showing terminal bifid branching (asterisks). (F) A primary bud arising from healthy donor-derived tubule cultured as that in (E). (G) Percentage of the ramified buds in the total buds emerged in healthy donor- and patient-derived tubules cultured with all growth factors. Data are expressed as means ± SEM from three independent experiments. Number of fields analyzed: $n = 22$ for healthy donor- and $n = 27$ for patient-derived tubules. $^{**}P < 0.0005$ by two-tailed Student's *t*-test. (H,I) Patient-derived tubule cultured with all growth factors shows mainly primary buds. (I) A primary bud arising from patient-derived tubule cultured as that in (H). DAPI, blue-stained nuclei; H, HGF; G, GDNF; F1, FGF1; F7, FGF7. Scale bars: 100 μm (B, left panel; E, left panel), 50 μm (E, right panel; H), 20 μm (B, right panel; C,F,I).

does not allow for the evaluation of important morphological changes that occur within the structure of the epithelial polycystic tubules, such as lumen obstruction and polarity perturbation, which would be crucial for reliably studying the pathogenesis of the disease and for testing drug efficacy. Unfortunately, there are currently no *in vitro* models that mimic cystogenesis *in vivo* closely enough to be an adequate alternative to traditional cell cultures. This, in combination with the lack of effective PKD therapies, makes the development of realistic PKD model systems an imperative task. Our system covers this methodological gap by allowing for efficient tubular cystogenesis *in vitro* and quantitative evaluation of drug effects on tubular cyst regression. In fact, when stimulated with forskolin, our engineered tubules developed numerous polarized cysts that were closely packed along the length of the tubules, obstructing the lumen, as happens in PKD *in vivo*. When we added Tolvaptan, OCTR, PAS, 2DG or berberine to the culture medium, cyst density within tubules decreased significantly to different extents, clearly indicating that engineered tubules can be an efficient tool for mimicking PKD and quantifying the effects

Fig. 5. Engineering functional human tubules using iPSCs. (A) Experimental design. Human iPSCs are differentiated toward UB-like progenitor cells. The 3- and 4-day differentiated cells are re-suspended in collagen, seeded into the PDMS scaffolds, and cultured in the presence of HGF and GDNF for 2 days. (B) A branch from 3-day differentiated cell-derived macrotubule displaying a continuous lumen (Lu) enclosed by a monolayer of E-cadherin (white) and WGA-lectin (green) positive cells. Inset: cells of the tubular wall show aligned nuclei (blue), and E-cadherin (white) and WGA-lectin (green) in the basolateral membranes. (C) Z-stack images of 4-day differentiated cell-derived microtubule endowed with a central lumen (Lu) lined by a WGA-lectin-positive (red) epithelium. (D) Three-dimensional reconstruction of z-stack images of an iPSC-derived microtubule labeled with WGA-lectin. Two distinct z-stack series of captures from the top of the tubule to its centre and from the top to the centre of the other side were reconstructed and merged into the 3D composite image. The dashed line indicates the plane of image merging. (E) Cross-section of engineered microtubule showing the lumen (Lu) enclosed by epithelial cells with aligned nuclei and positive for WGA-lectin. (F–L) iPSC-derived tubule cells express PAX2 (red) (F), HOXB7 (white) and Ret (red) (G,H, inset), Claudin 7 (red) (I,J) and GATA3 (red) (K,L). (M,N) Microtubules showing (M) dextran (green) and (N) 6CF (green) internalization. UB, ureteric bud; d, day; WGA-lectin, wheat germ agglutinin-lectin; PAX2, paired box 2; HOXB7, homeobox B7; Ret, ret proto-oncogene; GATA3, GATA binding protein 3; DAPI, blue-stained nuclei; 6CF, 6-carboxyfluorescein. Scale bars: 100 μm (B,C and M), 50 μm (N), 25 μm (E-L), x,y, 500 μm, and z, 100 μm (D).

of different pharmacological agents. Most importantly, we showed that 2DG and berberine had a robust effect on cyst regression and totally restored the central lumen and tubular integrity. These results highlight the clinical potential of 2DG, and point out the hitherto unknown therapeutic potential of berberine for PKD treatment.

We then demonstrated that our engineering system can also be adapted to model human PKD by constructing similar tubules using cells that were isolated from a patient with ADPKD and confirming the beneficial effects of 2DG and berberine. Previous studies have successfully derived iPSC lines from PKD patients [28, 72–74]. Moreover, Xia and colleagues showed that PKD-derived iPSCs can differentiate into UB progenitors and integrate into reaggregating mouse kidneys to form chimeric UB structures [28]. However, a 3D cellular model that can yield patient-derived cysts is still an unmet need in experimental nephrology. This can be attributed to a large extent to an inherent lack of reproducibility in iPSC-based technologies [75]. For example, pioneering studies in the field have generated a genetic model of PKD organoids [15, 16] using iPSCs and CRISPR/Cas9 technology, but the dramatic variability of iPSCs from patients in their abilities to form organoids [15] did not allow for the generation of patient-specific tissues. As a result, apart from some toxicity tests, no technology has so far been successful in testing therapeutic drug efficacy using patient-specific tissues. With our system, we here provide a novel technology that can efficiently model patient-specific PKD cystogenesis, and be used as a reliable and reproducible tool for preclinical drug testing.

The study of human developmental processes and disorders is currently limited by the scarcity of suitable human embryonic samples and the lack of methods for engineering *in vitro* kidney tissue from patients with genetic disorders. Significant progress in the field has been made with the development of organ-on-a-chip systems that can replicate some specific features of kidney development and functions, such as the formation of the glomerular filtration barrier [76]. However, these methods do not allow for studies into more complex developmental and morphogenetic processes, (*e.g.* UB branching and budding), which would be very useful for evaluating developmental disorders. Spurred on by these problems, we tested our system's ability to efficiently engineer human kidney tubules, using iPSCs previously directed to differentiate into UB-committed cells. By adding GDNF treatment to our original protocol we generated human tubular structures with monolayered epithelia and a lumen, and typical maturation characteristics of *in vitro* cultured UBs, such as macromolecule internalization and OAT-mediated transportation [46, 47, 77]. Human UB-like tubules also responded to embryonic kidney developmental cues to form primary and secondary buds, highlighting the utility of our system for studying mechanisms of human kidney development. Indeed, we used our system to identify a combination of growth factors to induce UB-like tubule budding, and show developmental defects in tubules derived from a patient carrying a heterozygous *PAX2* mutation. It is noteworthy that this patient was previously diagnosed with focal segmental glomerulosclerosis (FSGS) [67], which is commonly considered a disease of the podocytes. Our finding, though, suggests that *PAX2* mutations affect kidney development very early, even before the emergence of nephrons and podocytes. This is supported by data from heterozygous *Pax2* mutant mice showing that reduced UB branching is associated with a decrease in nephron numbers at birth [78]. It is possible that under conditions of impaired UB branching and reduced nephron numbers, FSGS lesions develop as a result of hemodynamic rearrangements, as commonly observed in patients with fewer nephrons at birth [79].

Although additional studies are needed to validate this hypothesis, our finding provides fresh insights in understanding the pathogenesis of FSGS, and confirms the utility of our system to study individual patient's genetic disorders, for which no models currently exist.

In summary, our engineering system offers three principal advances compared to previous organoid and engineering systems: i) our system can yield complex tubular structures with predefined dimensions and patterns, (ii) it presents exceptional robustness and reproducibility, as it can easily be optimized and adapted to different cell types and lines; in our study, we successfully engineered tubules using 1 canine cell line, 3 human iPSC clones, and primary cells from an ADPKD patient, (iii) it can yield patient-specific 3D kidney structures (from iPSCs or huADPKD cells) -which has so far been an unmet need in experimental nephrology- to model human genetic diseases, test drugs, and model human developmental disorders. In particular, the development of a patient-specific PKD model for testing drug efficacy provides an important methodological advance in the field, as it can be used for personalized drug testing and precision medicine applications.

Overall, this method provides an accurate, quick, cost-effective and reproducible system with which to model kidney disease and development, and possibly a promising platform from which the controlled generation of human kidney tissues can be optimized for regenerative medicine applications.

Supplementary data to this article can be found online at https://doi.org/10.1016/j.ebiom.2018.06.005.

Acknowledgements

The authors wish to thank Kerstin Mierke for excellent editing work on the manuscript and Fabio Sangalli for confocal image acquisition and composition, and technical IT support. We are also grateful to Rubina Novelli and Sara Conti for the valuable comments and suggestions in PKD models and microscopy analysis. Moreover, the authors would like to thank Andrea Remuzzi for providing the MDCK type II cells, Paola Rizzo for valuable technical assistance in cross-sectional histological analysis, Paolo Fruscella and Ursula Giussoni for performing the karyotype analysis, Andrea Volpe for help with 3D-printing, Valentina Mussi for substantial technical contributions, Giuseppe Firpo, Roberto Lo Savio and Luca Repetto for valuable comments on the design and fabrication of PDMS scaffold. We are also thankful to the patient L.S. for the kindly blood donation, and to Manuela Passera for helping with the submission of the manuscript.

Funding Sources

Valentina Benedetti and Valerio Brizi are recipients of fellowship from Fondazione Aiuti per la Ricerca sulle Malattie Rare (ARMR), Bergamo, Italy. This study was partially supported by the Associazione per la Ricerca sul Diabete Italia (ARDI), the European Research Council ERC-2010-AdG-268632 RESET Grant, European Commission grant no. HEALTH-F4-2012-305436 (STELLAR project) and grants from the Italian Ministry of Education, University and Research, Flagship Project Nanomax and FIRB project Newton RBAP11BYNP_003. The authors gratefully thank Bellco Srl for continued support.

Conflicts of Interest

None.

Author Contributions

C.X. conceived the strategy and supervised the project; P.G. devised the scaffold method and fabrication settings; P.G. and E.A. designed and developed PDMS scaffolds; C.X., V. Benedetti and V. Brizi designed and developed the 3D culture system; V. Brizi performed iPSC differentiation experiments and real time qRT-PCR; V. Benedetti and V. Brizi performed all 3D culture experiments, the functional studies, immunocytochemical analysis and hematoxylin and eosin staining; O.C. generated and characterized iPSCs from the patient and performed some real time qRT-PCR experiments; C.X., G.R.,V.Benedetti and V. Brizi analyzed the data; V. Benedetti, V. Brizi and P.G. drafted the manuscript; C.X. and V. Benedetti wrote the paper; S.T. supervised iPSC experiments; U.V. supervised fractal designs; G.R., A.B. and U.V. critically revised the paper.

V. Benedetti, V. Brizi and P.G. contributed equally.

References

[1] Astashkina A, Grainger DW. Critical analysis of 3-D organoid in vitro cell culture models for high-throughput drug candidate toxicity assessments. Adv Drug Deliv Rev 2014;69–70:1–18.
[2] Xinaris C, Brizi V, Remuzzi G. Organoid models and applications in biomedical research. Nephron 2015;130:191–9.
[3] Auerbach R, Grobstein C. Inductive interaction of embryonic tissues after dissociation and reaggregation. Exp Cell Res 1958;15:384–97.
[4] Xinaris C, Benedetti V, Rizzo P, Abbate M, Corna D, Azzollini N, et al. In vivo maturation of functional renal organoids formed from embryonic cell suspensions. J Am Soc Nephrol 2012;23:1857–68.
[5] Xinaris C, Benedetti V, Novelli R, Abbate M, Rizzo P, Conti S, et al. Functional human podocytes generated in organoids from amniotic fluid stem cells. J Am Soc Nephrol 2015;27(5):1400–11.
[6] Qiao J, Sakurai H, Nigam SK. Branching morphogenesis independent of mesenchymal-epithelial contact in the developing kidney. Proc Natl Acad Sci U S A 1999;96:7330–5.
[7] Steer DL, Bush KT, Meyer TN, Schwesinger C, Nigam SK. A strategy for in vitro propagation of rat nephrons. Kidney Int 2002;62:1958–65.
[8] Bryant DM, Datta A, Rodriguez-Fraticelli AE, Peranen J, Martin-Belmonte F, Mostov KE. A molecular network for de novo generation of the apical surface and lumen. Nat Cell Biol 2010;12:1035–45.
[9] Montesano R, Matsumoto K, Nakamura T, Orci L. Identification of a fibroblast-derived epithelial morphogen as hepatocyte growth factor. Cell 1991;67:901–8.
[10] Pollack AL, Runyan RB, Mostov KE. Morphogenetic mechanisms of epithelial tubulogenesis: MDCK cell polarity is transiently rearranged without loss of cell-cell contact during scatter factor/hepatocyte growth factor-induced tubulogenesis. Dev Biol 1998;204:64–79.
[11] Sakurai H, Barros EJ, Tsukamoto T, Barasch J, Nigam SK. An in vitro tubulogenesis system using cell lines derived from the embryonic kidney shows dependence on multiple soluble growth factors. Proc Natl Acad Sci U S A 1997;94:6279–84.
[12] Santos OF, Barros EJ, Yang XM, Matsumoto K, Nakamura T, Park M, et al. Involvement of hepatocyte growth factor in kidney development. Dev Biol 1994;163:525–9.
[13] Ye P, Habib SL, Ricono JM, Kim NH, Choudhury GG, Barnes JL, et al. Fibronectin induces ureteric bud cells branching and cellular cord and tubule formation. Kidney Int 2004;66:1356–64.
[14] Astashkina AI, Mann BK, Prestwich GD, Grainger DW. Comparing predictive drug nephrotoxicity biomarkers in kidney 3-D primary organoid culture and immortalized cell lines. Biomaterials 2012;33:4712–21.
[15] Cruz NM, Song X, Czerniecki SM, Gulieva RE, Churchill AJ, Kim YK, et al. Organoid cystogenesis reveals a critical role of microenvironment in human polycystic kidney disease. Nat Mater 2017;16:1112–9.
[16] Freedman BS, Brooks CR, Lam AQ, Fu H, Morizane R, Agrawal V, et al. Modelling kidney disease with CRISPR-mutant kidney organoids derived from human pluripotent epiblast spheroids. Nat Commun 2015;6:8715.
[17] Morizane R, Lam AQ, Freedman BS, Kishi S, Valerius MT, Bonventre JV. Nephron organoids derived from human pluripotent stem cells model kidney development and injury. Nat Biotechnol 2015;33(11):1193–200.
[18] Taguchi A, Kaku Y, Ohmori T, Sharmin S, Ogawa M, Sasaki H, et al. Redefining the in vivo origin of metanephric nephron progenitors enables generation of complex kidney structures from pluripotent stem cells. Cell Stem Cell 2014;14:53–67.
[19] Takasato M, Er PX, Chiu HS, Maier B, Baillie GJ, Ferguson C, et al. Kidney organoids from human iPS cells contain multiple lineages and model human nephrogenesis. Nature 2015;526(7574):564–8.
[20] Mae S-I, Ryosaka M, Toyoda T, Matsuse K, Oshima Y, Tsujimoto H, et al. Generation of branching ureteric bud tissues from human pluripotent stem cells. Biochem Biophys Res Commun 2018;495:954–61.
[21] Taguchi A, Nishinakamura R. Higher-order kidney organogenesis from pluripotent stem cells. Cell Stem Cell 2017;21:730–746.e6.
[22] Angeli E, Volpe A, Fanzio P, Repetto L, Firpo G, Guida P, et al. Simultaneous electro-optical tracking for nanoparticle recognition and counting. Nano Lett 2015;15:5696–701.
[23] McDonald JC, Whitesides GM. Poly(dimethylsiloxane) as a material for fabricating microfluidic devices. Acc Chem Res 2002;35:491–9.
[24] Park JY, Ahn D, Choi YY, Hwang CM, Takayama S, Lee SH, et al. Surface chemistry modification of PDMS elastomers with boiling water improves cellular adhesion. Sens Actuators B Chem 2012;173:765–71.
[25] Valamehr B, Jonas SJ, Polleux J, Qiao R, Guo S, Gschweng EH, et al. Hydrophobic surfaces for enhanced differentiation of embryonic stem cell-derived embryoid bodies. Proc Natl Acad Sci U S A 2008;105:14459–64.
[26] Ciampi O, Iacone R, Longaretti L, Benedetti V, Graf M, Magnone MC, et al. Generation of functional podocytes from human induced pluripotent stem cells. Stem Cell Res 2016;17:130–9.
[27] Imberti B, Tomasoni S, Ciampi O, Pezzotta A, Derosas M, Xinaris C, et al. Renal progenitors derived from human iPSCs engraft and restore function in a mouse model of acute kidney injury. Sci Rep 2015;5:8826.
[28] Xia Y, Nivet E, Sancho-Martinez I, Gallegos T, Suzuki K, Okamura D, et al. Directed differentiation of human pluripotent cells to ureteric bud kidney progenitor-like cells. Nat Cell Biol 2013;15:1507–15.
[29] Colom A, Galgoczy R, Almendros I, Xaubet A, Farré R, Alcaraz J. Oxygen diffusion and consumption in extracellular matrix gels: implications for designing three-dimensional cultures. J Biomed Mater Res A 2014;102:2776–84.
[30] Li H, Findlay IA, Sheppard DN. The relationship between cell proliferation, Cl- secretion, and renal cyst growth: a study using CFTR inhibitors. Kidney Int 2004;66:1926–38.
[31] Masyuk TV, Radtke BN, Stroope AJ, Banales JM, Gradilone SA, Huang B, et al. Pasireotide is more effective than octreotide in reducing hepatorenal cystogenesis in rodents with polycystic kidney and liver diseases. Hepatology 2013;58:409–21.
[32] Riwanto M, Kapoor S, Rodriguez D, Edenhofer I, Segerer S, Wüthrich RP. Inhibition of aerobic glycolysis attenuates disease progression in polycystic kidney disease. PloS One 2016;11:e0146654.
[33] Bonon A, Mangolini A, Pinton P, Del Senno L, Aguiari G. Berberine slows cell growth in autosomal dominant polycystic kidney disease cells. Biochem Biophys Res Commun 2013;441:668–74.
[34] de Stephanis L, Bonon A, Varani K, Lanza G, Gafà R, Pinton P, et al. Double inhibition of cAMP and mTOR signalling may potentiate the reduction of cell growth in ADPKD cells. Clin Exp Nephrol 2017;21:203–11.
[35] Reif GA, Yamaguchi T, Nivens E, Fujiki H, Pinto CS, Wallace DP. Tolvaptan inhibits ERK-dependent cell proliferation, cl^- secretion, and in vitro cyst growth of human ADPKD cells stimulated by vasopressin. Am J Physiol Renal Physiol 2011;301:F1005–13.
[36] Gao J, Zhou H, Lei T, Zhou L, Li W, Li X, et al. Curcumin inhibits renal cyst formation and enlargement in vitro by regulating intracellular signaling pathways. Eur J Pharmacol 2011;654:92–9.
[37] Lin Y, Zhang S, Tuukkanen J, Peltoketo H, Pihlajaniemi T, Vainio S. Patterning parameters associated with the branching of the ureteric bud regulated by epithelial-mesenchymal interactions. Int J Dev Biol 2003;47:3–13.
[38] Pons BE. Generalized self-contacting symmetric fractal trees. Symmetry Cult Sci 2013;21:333–51.
[39] Taylor TD. Golden Fractal Trees. In: Sarhangi R, Barallo J, editors. Proceedings of the 2007 bridges conference on mathematical connections in art, music, and science; 2007. p. 181–8.
[40] Andrew DJ, Ewald AJ. Morphogenesis of epithelial tubes: insights into tube formation, elongation, and elaboration. Dev Biol 2010;341:34–55.
[41] Prozialeck WC, Lamar PC, Appelt DM. Differential expression of E-cadherin, N-cadherin and beta-catenin in proximal and distal segments of the rat nephron. BMC Physiol 2004;4:10.
[42] Schumacher KM, Phua SC, Schumacher A, Ying JY. Controlled formation of biological tubule systems in extracellular matrix gels in vitro. Kidney Int 2008;73:1187–92.
[43] Meder D, Shevchenko A, Simons K, Fullekrug J. Gp135/podocalyxin and NHERF-2 participate in the formation of a preapical domain during polarization of MDCK cells. J Cell Biol 2005;168:303–13.
[44] Datta A, Bryant DM, Mostov KE. Molecular regulation of lumen morphogenesis. Curr Biol CB 2011;21:R126–36.
[45] Zegers MM. 3D in vitro cell culture models of tube formation. Semin Cell Dev Biol 2014;31:132–40.
[46] Meyer TN, Schwesinger C, Bush KT, Stuart RO, Rose DW, Shah MM, et al. Spatiotemporal regulation of morphogenetic molecules during in vitro branching of the isolated ureteric bud: toward a model of branching through budding in the developing kidney. Dev Biol 2004;275:44–67.
[47] Sweet DH, Eraly SA, Vaughn DA, Bush KT, Nigam SK. Organic anion and cation transporter expression and function during embryonic kidney development and in organ culture models. Kidney Int 2006;69:837–45.
[48] Nagle MA, Truong DM, Dnyanmote AV, Ahn S-Y, Eraly SA, Wu W, et al. Analysis of three-dimensional systems for developing and mature kidneys clarifies the role of OAT1 and OAT3 in antiviral handling. J Biol Chem 2011;286:243–51.
[49] Ong AC, Devuyst O, Knebelmann B, Walz G. Autosomal dominant polycystic kidney disease: the changing face of clinical management. Lancet 2015;385:1993–2002.
[50] Su L, Liu L, Jia Y, Lei L, Liu J, Zhu S, et al. Ganoderma triterpenes retard renal cyst development by downregulating Ras/MAPK signaling and promoting cell differentiation. Kidney Int 2017;92:1404–18.
[51] Serra AL, Poster D, Kistler AD, Krauer F, Raina S, Young J, et al. Sirolimus and kidney growth in autosomal dominant polycystic kidney disease. N Engl J Med 2010;363:820–9.
[52] Blair HA, Keating GM. Tolvaptan: a review in autosomal dominant polycystic kidney disease. Drugs 2015;75:1797–806.
[53] Chiaravalli M, Rowe I, Mannella V, Quilici G, Canu T, Bianchi V, et al. 2-deoxy-d-glucose ameliorates PKD progression. J Am Soc Nephrol JASN 2016;27:1958–69.
[54] Sun Y, Xun K, Wang Y, Chen X. A systematic review of the anticancer properties of berberine, a natural product from Chinese herbs. Anticancer Drugs 2009;20:757–69.
[55] Caroli A, Antiga L, Conti S, Sonzogni A, Fasolini G, Ondei P, et al. Intermediate volume on computed tomography imaging defines a fibrotic compartment that predicts glomerular filtration rate decline in autosomal dominant polycystic kidney disease patients. Am J Pathol 2011;179:619–27.
[56] Grantham JJ, Mulamalla S, Swenson-Fields KI. Why kidneys fail in autosomal dominant polycystic kidney disease. Nat Rev Nephrol 2011;7:556–66.
[57] Shakya R, Watanabe T, Costantini F. The role of GDNF/Ret signaling in ureteric bud cell fate and branching morphogenesis. Dev Cell 2005;8:65–74.
[58] Yang Z, Zimmerman S, Brakeman PR, Beaudoin GM, Reichardt LF, Marciano DK. De novo lumen formation and elongation in the developing nephron: a central role for afadin in apical polarity. Dev Camb Engl 2013;140:1774–84.
[59] Michos O. Kidney development: from ureteric bud formation to branching morphogenesis. Curr Opin Genet Dev 2009;19:484–90.
[60] Paroly SS, Wang F, Spraggon L, Merregaert J, Batourina E, Tycko B, et al. Stromal protein Ecm1 regulates ureteric bud patterning and branching. PloS One 2013;8:e84155.
[61] Wang S, Sekiguchi R, Daley WP, Yamada KM. Patterned cell and matrix dynamics in branching morphogenesis. J Cell Biol 2017;216:559–70.
[62] Barros EJ, Santos OF, Matsumoto K, Nakamura T, Nigam SK. Differential tubulogenic and branching morphogenetic activities of growth factors: implications for epithelial tissue development. Proc Natl Acad Sci U S A 1995;92:4412–6.

[63] Qiao J, Uzzo R, Obara-Ishihara T, Degenstein L, Fuchs E, Herzlinger D. FGF-7 modulates ureteric bud growth and nephron number in the developing kidney. Dev Camb Engl 1999;126:547–54.
[64] Qiao J, Bush KT, Steer DL, Stuart RO, Sakurai H, Wachsman W, et al. Multiple fibroblast growth factors support growth of the ureteric bud but have different effects on branching morphogenesis. Mech Dev 2001;109:123–35.
[65] Dressler GR, Woolf AS. Pax2 in development and renal disease. Int J Dev Biol 1999; 43:463–8.
[66] Harshman LA, Brophy PD. PAX2 in human kidney malformations and disease. Pediatr Nephrol Berl Ger 2012;27:1265–75.
[67] Barua M, Stellacci E, Stella L, Weins A, Genovese G, Muto V, et al. Mutations in PAX2 associate with adult-onset FSGS. J Am Soc Nephrol JASN 2014;25:1942–53.
[68] Eccles MR, He S, Legge M, Kumar R, Fox J, Zhou C, et al. PAX genes in development and disease: the role of PAX2 in urogenital tract development. Int J Dev Biol 2002; 46:535–44.
[69] Balcarova-Ständer J, Pfeiffer SE, Fuller SD, Simons K. Development of cell surface polarity in the epithelial Madin-Darby canine kidney (MDCK) cell line. EMBO J 1984;3: 2687–94.
[70] Kadono Y, Shibahara K, Namiki M, Watanabe Y, Seiki M, Sato H. Membrane type 1-matrix metalloproteinase is involved in the formation of hepatocyte growth factor/scatter factor-induced branching tubules in madin-darby canine kidney epithelial cells. Biochem Biophys Res Commun 1998;251:681–7.
[71] Mangoo-Karim R, Uchic M, Lechene C, Grantham JJ. Renal epithelial cyst formation and enlargement in vitro: dependence on cAMP. Proc Natl Acad Sci U S A 1989; 86:6007–11.
[72] Freedman BS, Lam AQ, Sundsbak JL, Iatrino R, Su X, Koon SJ, et al. Reduced ciliary polycystin-2 in induced pluripotent stem cells from polycystic kidney disease patients with PKD1 mutations. J Am Soc Nephrol JASN 2013;24:1571–86.
[73] Huang C-Y, Ho M-C, Lee J-J, Hwang D-Y, Ko H-W, Cheng Y-C, et al. Generation of induced pluripotent stem cells derived from an autosomal dominant polycystic kidney disease patient with a p.Ser1457fs mutation in PKD1. Stem Cell Res 2017;24:139–43.
[74] Thatava T, Armstrong AS, De Lamo JG, Edukulla R, Khan YK, Sakuma T, et al. Successful disease-specific induced pluripotent stem cell generation from patients with kidney transplantation. Stem Cell Res Ther 2011;2:48.
[75] Huch M, Knoblich JA, Lutolf MP, Martinez-Arias A. The hope and the hype of organoid research. Dev Camb Engl 2017;144:938–41.
[76] Musah S, Mammoto A, Ferrante TC, Jeanty SSF, Hirano-Kobayashi M, Mammoto T, et al. Mature induced-pluripotent-stem-cell-derived human podocytes reconstitute kidney glomerular-capillary-wall function on a chip. Nat Biomed Eng 2017;1.
[77] Lawrence ML, Chang CH, Davies JA. Transport of organic anions and cations in murine embryonic kidney development and in serially-reaggregated engineered kidneys. Sci Rep 2015;5:9092.
[78] Dziarmaga A, Eccles M, Goodyer P. Suppression of ureteric bud apoptosis rescues nephron endowment and adult renal function in Pax2 mutant mice. J Am Soc Nephrol JASN 2006;17:1568–75.
[79] Luyckx VA, Perico N, Somaschini M, Manfellotto D, Valensise H, Cetin I, et al. A developmental approach to the prevention of hypertension and kidney disease: a report from the Low Birth Weight and Nephron Number Working Group. Lancet Lond Engl 2017;390(10092):424–8.